IDENTIFYING ANTI-CANCER DRUGS TARGETING ALK INHIBITORS WITH P-GLYCOPROTEIN AND STUDYING IT'S MOLECULAR MECHANISM OF TRANSPORT

by

AMEENA HUSSAIN AHMED

(Under the Direction of Arthur Roberts)

ABSTRACT

The P-glycoprotein transporter is important for drug disposition because it effluxes a wide variety of chemicals from cells via conformational changes and ATP hydrolysis. A variety of medicines have been shown to stimulate Pgp ATP hydrolysis, although the relationship between ATP and drug binding is unclear. This work focuses on investigating the structural differences between three anticancer drugs, ceritinib, crizotinib and alectinib with Pgp. Results of this research demonstrated that these drugs stimulated the ATPase activity with mouse Pgp, alectinib has a much lower K_m of the Pgp-mediated ATP hydrolysis than both crizotinib and ceritinib. However the KDs (dissociation constants) of ceritinib and crizotinib determined by fluorescence did not have a significant difference and they were relatively similar. These anticancer drugs move Pgp to an "open" conformation, however in the presence of AMP-PNP ceritinib and alectinib shifted towards a "intermediate" confirmation whereas crizotinib had little effect according to acrylamide quenching.

IDENTIFYING ANTI-CANCER DRUGS TARGETTING ALK INHIBITORS WITH P-GLYCOPROTEIN AND STUDYING IT'S MOLECULAR MECHANISM OF TRANSPORT

By

AMEENA HUSSAIN AHMED

B.S., UAE University, 2018

A Thesis Submitted to the Graduate Faculty of The University of Georgia in Partial Fulfillment of the Requirements for the Degree

MASTER OF SCIENCE

ATHENS, GEORGIA

2021

IDENTIFYING ANTI-CANCER DRUGS TARGETTING ALK INHIBITORS WITH P-GLYCOPROTEIN AND STUDYING IT'S MOLECULAR MECHANISM OF TRANSPORT

by

AMEENA HUSSAIN AHMED

Major Professor: Arthur Roberts

Committee: George Zheng
Neil Grimsey

Electronic version approved:

Ron Walcott
Vice Provost for Graduate Education and Dean of the Graduate School
The University of Georgia
December 2021

TABLE OF CONTENTS

LIST OF TABLES

LIST OF FIGURES

Page

CHAPTER 1

INTRODUCTION

NSCLC (non-small cell lung cancer) is the most prevalent form of lung cancer, accounting for almost half of all cases accounting to 84% of all lung cancer cases and it is a kind of epithelial lung cancer that is not the same as small cell lung cancer. The most frequent types of NSCLC are squamous cell carcinoma, large cell carcinoma, and adenocarcinoma, while there are many additional types that are less common, and all types can have uncommon histologic variants. NSCLCs are relatively unresponsive to chemotherapy and radiation therapy when compared to SCLCs (small cell lung cancer).

Patients with minor illnesses can be treated with anesthetic or procedures combined with chemotherapy. Local regulation can be achieved with radiation therapy for a large number of patients with unresectable disorders, it can only be cured in a small percentage of cases. “In 2021, an estimated 235,760 adults (119,100 men and 116,660 women) in the United States will be diagnosed with lung cancer. However, since the mid-2000s, incidence rates have dropped by around 2% each year.”[1]

Lung cancer is 15 percent more common in black males than in white men. When compared to white women, black women had a 14 percent lower risk of lung cancer. The illness is more likely to strike those over the age of 65. The average age at which a person is diagnosed is 70. Lung cancer is the second most prevalent cancer in men and women and the main cause of cancer mortality.

[1] “Lung Cancer - Non-Small Cell - Statistics.”

"It is estimated that 131,880 (69,410 men and 62,470 women) deaths from this disease will occur this year."[2] We now live in an era in which many patients with lung cancer are treated in a way that is very targeted and matched to the genetic cause of that disease but the major challenge is that despite the improvement in the way that we think of lung cancer and treat lung cancer patients we are still not curing many patients due to its developing multi drug resistance making drug treatment very difficult. One well studied protein identified to play a major role in multi drug resistance is p-glycoprotein 1(p-gp).[3]

Tumors were discovered to be capable of acquiring resistance to a wide spectrum of cytotoxic drugs during cancer treatment (multidrug resistance). The concept of multidrug resistance was later studied using drug-resistant mammalian cell lines. Cell lines chosen for resistance to one cytotoxic agent were later discovered to have cross-resistance to other structurally unrelated cytotoxic drugs. When compared to drug-sensitive parent cell lines, the drug-resistant cell lines almost always overexpressed a 170 kDa glycosylated plasma membrane protein.

P-glycoprotein (P-gp) appeared to influence the membrane's permeability to cytotoxic chemicals[4]. P-gp was later discovered to be an ATP-dependent drug pump capable of transporting a wide range of structurally unrelated substances out of the cell.

[2] "Lung Cancer - Non-Small Cell - Statistics."
[3] "P-Glycoprotein - an Overview | ScienceDirect Topics."
[4] Juliano and Ling, "A Surface Glycoprotein Modulating Drug Permeability in Chinese Hamster Ovary Cell Mutants."

1.1 Background information on P-glycoprotein

P-glycoprotein is a plasma membrane protein as well as a multidrug resistance protein also known as MDR1 or ABCB1 that can pump a wide variety of cytotoxic compounds out of cells, the overexpression of this protein can lead to multidrug resistance during chemotherapy. It is very important in chemotherapy since it can prevent the accumulation of many anti-cancer medications in cells, resulting in multidrug resistance(MDR). Since its discovery more than three decades ago, P-gp has been a focus for better cancer treatment. The transporter is expressed at relatively high concentrations in the liver, brain, placenta, kidneys and brain. P-gp is an ABC transporter that needs the energy from ATP binding and hydrolysis in the nucleotide binding domains(NBDs) to drive the transport across the membrane.[5]

P-gp is divided into two halves, each with six transmembrane segments and a nucleotide domain, when the two halves are expressed separately, they produce an inactive transporter, but when they are co-expressed in the same cell they form an active transporter. The two halves form two wings. One wing consists of NBD1 and transmembrane (TM) segments 1, 2, 3, 6, 10 and 11 while the other consists of NBD2 and TMs 4 5, 7, 8, 9 and 12.[6] Whereas the structure and function of NBDs are similar throughout families, transmembrane domains(TMDs) are highly heterogeneous, allowing transporters to recognize diverse substrates and use the energy from ATP hydrolysis to translocate molecules across membranes, irrespective of the prevailing concentration gradient.[7]

[5] "A Gene Optimization Strategy That Enhances Production of Fully Functional P-Glycoprotein in Pichia Pastoris."
[6] "A Gene Optimization Strategy That Enhances Production of Fully Functional P-Glycoprotein in Pichia Pastoris."
[7] Robey et al., "Revisiting the Role of ABC Transporters in Multidrug-Resistant Cancer."

While the energy from ATP can assist in the translocation of engaged ATP hydrolysis in the absence of substrates causes a conformation that is always altering may make MDR1 binding and trafficking easier a diverse set of substrates. Inhibitors may compete with drug binding at the drug binding sites which can prohibit transport activity where P-gp can alternate between and inward-facing, drug binding competent conformation with the TMDs that is open to the cytoplasm and an outwards-facing, drug releasing conformation with the TMDs accessible to the extracellular space[8].

It has been shown previously how the interactions between bound inhibitors and the drug binding site residues were initially seen in co-crystal structures with two inhibitors. However, additional research is needed to completely comprehend P-gp's interactions with medicines and inhibitors, as well as the molecular process of drug export. Large-scale manufacturing of the fully functioning protein is required for these activities.

1.2 Structure and mechanism of p-glycoprotein

ABC transporters consist of two cytoplasmic nucleotide-binding domains(NBDs) that bind and hydrolyze ATP and two transmembrane domains(TMDs) that recognize and transport substrates. TMDs are very heterogeneous, allowing transporters to detect a wide range of substrates and translocate molecules across membranes using the energy released by ATP hydrolysis, regardless of the concentration gradient. P-gp/MDR1 is made up of 1276–1280 amino acids and has a molecular mass of 170 kDa.

The most widely accepted topologic structure of P-gp/MDR1 is a tandemly duplicated structure with a nucleotide-binding domain (NBD) in either half of the molecule, revealing six anticipated and extremely hydrophobic transmembrane domains (TMDs)(figure 1)[9]. TMDs are

[8] Gutmann et al., "Understanding Polyspecificity of Multidrug ABC Transporters."
[9] Shilling et al., "New Light on Multidrug Binding by an ATP-Binding-Cassette Transporter."

thought to be the method by which drug molecules pass across the membrane. The NBDs, as well as the NH2- and COOH-termini, are intracellular, and the first extracellular loop is N-glycosylated. Each NBD is made up of two fundamental consensus motifs known as the Walker A and B motifs, as well as an ABC transporter S signature.

These motifs can be found in a wide variety of ATPases and are directly engaged in nucleotide-binding and hydrolysis. A highly charged 'linker region, which is phosphorylated at numerous locations by protein kinase C, separates the two half molecules.

P-gp/MDR1 has been found in a variety of topological orientations, and various investigations have found that conformational changes in the structure of P-gp during nucleotide binding result in changes in epitope accessibility, protease susceptibility, drug binding, fluorescence, and spectroscopic characteristics measurements. This conformational change allows access from the lipid bilayer to the central pore by opening one side of the pore throughout the depth of the lipid bilayer.

The two-dimensional projection maps for P-gp trapped at various stages of the hydrolytic cycle also show significant conformational changes at the extracellular face of the TMDs upon binding of the non-hydrolysable ATP analogue adenylyl-imidodiphosphate and after vanadate-trapping in the presence of adenosine diphosphate (ADP/Vi state)[10]. P-gp has been effectively overexpressed, purified, and reconstituted to obtain biological material for the transporter's structural resolution. Using electron cryomicroscopy, this effort yielded low-resolution structures. Early research found a substantial chamber associated with the NBDs on the inner surface of a 25-electron-microscopy structure. Further investigation of P-gp trapped in

[10] Zhou, "Structure, Function and Regulation of P-Glycoprotein and Its Clinical Relevance in Drug Disposition."

various catalytic states revealed substantial changes in the protein's TMDs[11]. These findings are the sole structural information available for any mammalian ABC transporter. The atomic intricacies of the substrate binding domains and the dynamics of the transport mechanism, on the other hand, are still unknown. Despite this, the atomic structure of P-gp or any other ATP-dependent multidrug transporter has yet to be determined.

[11] Rosenberg et al., "Three-Dimensional Structures of the Mammalian Multidrug Resistance P-Glycoprotein Demonstrate Major Conformational Changes in the Transmembrane Domains upon Nucleotide Binding *."

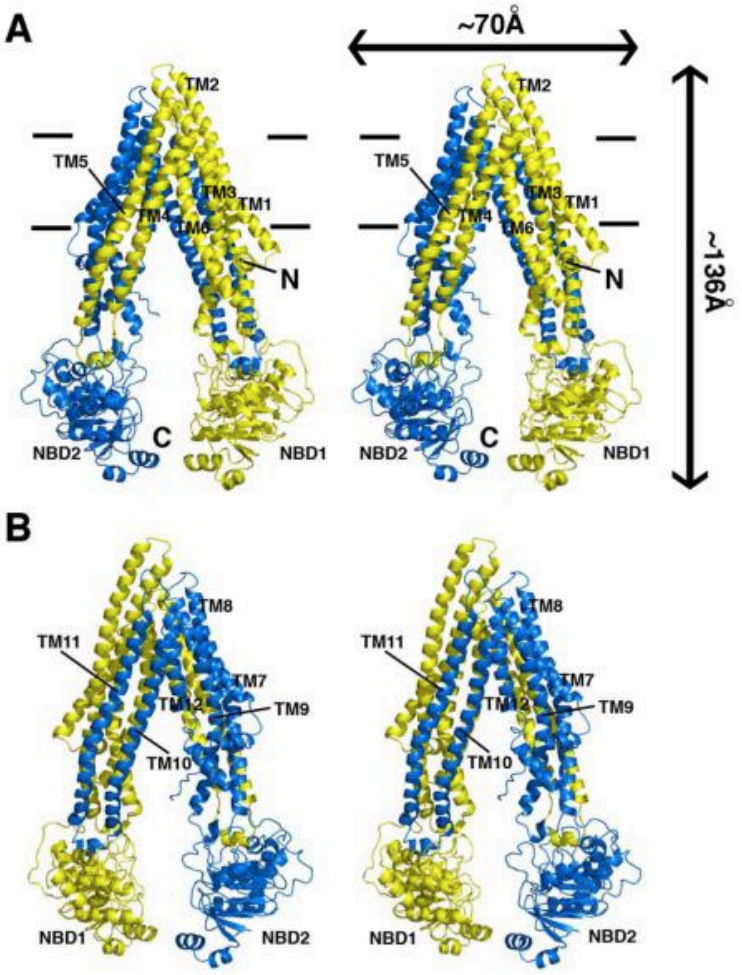

Figure 1: Structure of Pgp. (A) Front and (B) back stereo views of PGP. TM1-12 are labeled. The Nand C-terminal half of the molecule is colored yellow and blue, respectively. TM4-5 and TM10-11 cross over to form intertwined interfaces that stabilize the inward facing conformation. Horizontal bars represent the approximate positioning of the lipid bilayer. The N-and C-termini are labeled in panel A. Transmembrane (TM) domains and nucleotide binding domains (NBD) are also labeled.

*Note: Reprinted from Ling, V. (2009). Faculty opinions recommendation of structure of P-glycoprotein reveals a molecular basis for poly-specific drug binding. *Faculty Opinions – Post-Publication Peer Review of the Biomedical Literature*. https://doi.org/10.3410/f.1158560.618749

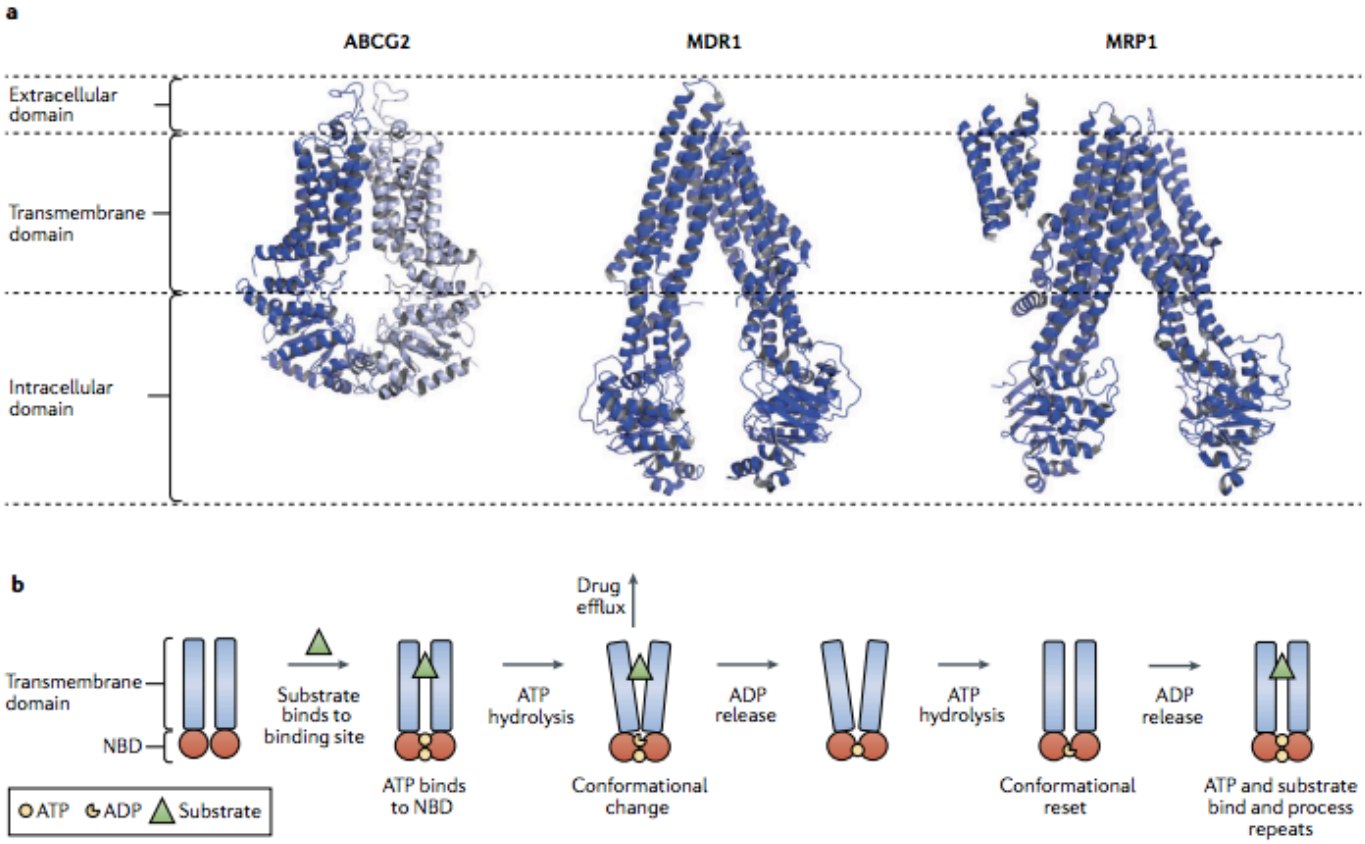

Figure 2: structure and mechanism of three ABC transporters
a | High resolution 3D structures of ATP-binding cassette (ABC) subfamily G member 2 (ABCG2)25 (PDB ID 5NJ3), multidrug resistance protein 1 (MDR1)23 (PDB ID 5KPI) and multidrug resistance-associated protein 1 (MRP1)24 (PDB ID 5UJ9). Although the structure for MRP1 is that of Bos taurus, the protein identity is 91%, and the structure is likely similar to that of human MRP1. Structures were generated using PyMol138 with data from RCSBPDB (see Related links). b | Schematic representation of the proposed pumping action of MDR1. The substrate binds to the binding pocket, and ATP binds to the two binding sites in the nucleotide-binding domains (NBDs). This is followed by the hydrolysis of ATP, which generates a conformational change, allowing the substrate to be released from the protein. The second molecule of ATP is hydrolysed, allowing for a conformational reset where substrate and ATP can bind again so the process can repeat.

*Note: Reprinted from Awad, M. M., & Shaw, A. T. (2014, July). *ALK inhibitors in non-small cell lung cancer: Crizotinib and beyond*. Clinical advances in hematology & oncology : H&O. Retrieved October 10, 2021, from https://www.ncbi.nlm.nih.gov/pmc/articles/PMC4215402/#R6.

1.3 ATP-binding domains

Both NBDs are required for P-gp/MDR1 to operate properly, and P-gp/MDR1 action is fully dependent on the presence of ATP. The ATP-binding domains function as an ATPase, converting ATP to ADP to give energy for P-gp/MDR1 to pump substrates across membranes, typically despite steep concentration gradients. To allow the full P-gp protein to function, ATP

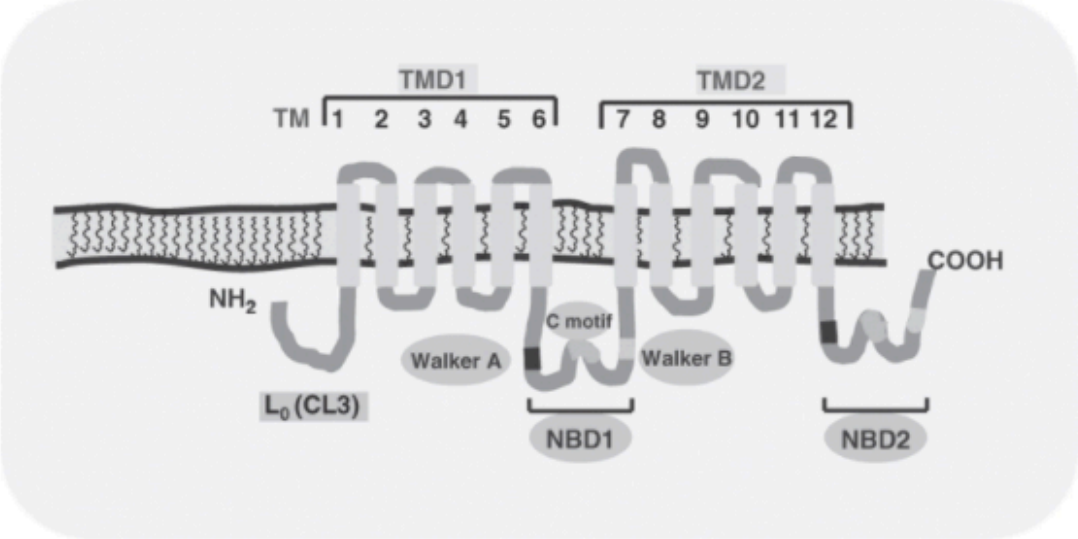

Figure 3: topology of P-glycoprotein.

must bind to both NBDs. However, whether hydrolysis of both bound ATP molecules is required to create activity is unknown. ATP binding, rather than ATP hydrolysis, causes major conformational changes in P-gp/MDR1.

Although it is commonly considered that ATP hydrolysis drives the transport mechanism, studies reveal that ATP binding, not hydrolysis, is responsible for drug binding affinity decreases to P-gp/MDR1. Thus, it appears that ATP binding causes substantial conformational changes in the transporter molecule that diminish drug binding affinity and expose the drug binding site to the extracellular milieu (central aqueous pore); ATP hydrolysis may simply ‘reset' the transporter

protein. Evidence suggests that P-gp/MDR1 has multiple binding sites divided evenly into two categories: transport and regulation[12].

P-gp/MDR1 has binding sites on both the N- and C-terminal portions, and these two sites may form a single region in the overall protein structure. The large spectrum of substances known to interact with P-gp/MDR1 could be explained by the presence of several drug binding sites on this protein. Previous research has discovered that P-gp/MDR1 has two primary substrate binding sites: TMD sites 5 and 6 and TMD sites 11 and 12[13].

All P-gp/MDR1 binding sites, as well as modulators regulating their function from transporting sites, appear to be able to transition between high- and low-affinity conformations. Stimuli such as substrate binding and/or ATP hydrolysis could trigger this. 2H/H-exchange kinetics, proteolytic accessibility, and alterations in antibody epitope recognition have all been used to indicate conformational changes in P-gp/MDR1. The molecular mechanism of substrate recognition, binding, and transport by P-gp/MDR1 must be elucidated. This knowledge could lead to the creation of new medications that avoid P-gp/MDR1 detection. In addition, novel medicines that bind strongly to P-gp/MDR1 and inactivate it could be developed. Various ALK inhibitors like Crizotinib, Ceritinib and Alectinib have been reported to reverse MDR by inhibiting the function of ABCB1.

1.4 The relationship between ATP hydrolysis and drug efflux

Purified hamster P-gp can actively create a 5.6-fold concentration gradient of colchicine in reconstituted lipid vesicles, demonstrating that P-gp has the capacity to efflux drug substrates

[12] Macdonald and Gledhill, "Potential Impact of ABCB1 (p-Glycoprotein) Polymorphisms on Avermectin Toxicity in Humans."
[13] Wang et al., "Structure–Activity Relationship."

out of the lipid bilayer[14]. P-gp could also transport spin-labeled verapamil into vesicles, generating a 13-fold gradient between the luminal and aqueous phases[15]. It has been suggested that human P-gp ATP sites are not similar rather considered asymmetric [16]. The fact that the NH2- and COOH- portions of P-gp were differently tagged with [∝- 32P]-8-azido-ATP led to this result. These investigations, however, had technical issues since the amount of ATP utilized and the amount of photo-cleavage achieved (about 10%) were substoichiometric. In the absence of any drug substrate, P-gp has a low baseline ATPase activity[17]**.** Phosphatidylcholine, phosphatidylethanolamine, phosphatidylserine, and sphingomyelin are all lipids that P-gp has been shown to transport in several investigations[18]. Thermodynamic experiments on P-gp, on the other hand, show that the protein's baseline ATPase activity is not related to the transport of an endogenous lipid[19].

Studies of disulfide cross-linking [20], fluorescence resonance energy transfer (FRET)[21], and cryo-electron imaging[22] of P-gp indicate that the two catalytic sites are near to each other. Cross-linking the endogenous cysteine residue inside each Walker can reveal such close closeness. As a result, it seems that the two ATP molecules bond at the interface between the two

[14] Sharom, Yu, and Doige, "Functional Reconstitution of Drug Transport and ATPase Activity in Proteoliposomes Containing Partially Purified P-Glycoprotein."
[15] Omote and Al-Shawi, "A Novel Electron Paramagnetic Resonance Approach to Determine the Mechanism of Drug Transport by P-Glycoprotein."
[16] Hrycyna et al., "Mechanism of Action of Human P-Glycoprotein ATPase Activity."
[17] Sarkadi et al., "Expression of the Human Multidrug Resistance CDNA in Insect Cells Generates a High Activity Drug-Stimulated Membrane ATPase."
[18] Romsicki and Sharom, "Phospholipid Flippase Activity of the Reconstituted P-Glycoprotein Multidrug Transporter."
[19] Al-Shawi et al., "Transition State Analysis of the Coupling of Drug Transport to ATP Hydrolysis by P-Glycoprotein."
[20] Loo and Clarke, "Drug-Stimulated ATPase Activity of Human P-Glycoprotein Is Blocked by Disulfide Cross-Linking between the Nucleotide-Binding Sites*."
[21] Qu and Sharom, "FRET Analysis Indicates That the Two ATPase Active Sites of the P-Glycoprotein Multidrug Transporter Are Closely Associated."
[22] Lee et al., "Projection Structure of P-Glycoprotein by Electron Microscopy. Evidence for a Closed Conformation of the Nucleotide Binding Domains."

NBDs. The signature sequences of several bacterial ABC-type proteins, including the DNA repair enzyme Rad50, the bacterial vitamin B12 transporter BtuCD, the bacterial lipid transporter MsbA, and the inactive NBD of Methanococcus jannaschii MJ0796, are also close to the Walker A sites.

Several groups have utilized biochemical techniques to prove that conformational changes are caused by ATP hydrolysis rather than nucleotide binding. However, cryo-electron imaging of P-gp reveals that when AMP-PNP is bound has the potential to generate significant conformational alterations in TMDs[23]. Both ATP binding and hydrolysis have the potential to trigger different conformational changes in TMDs. The labeling of residues in the drug-binding pocket can be affected by nucleotide binding and vanadate trapping of nucleotides by P-gp.

As a result, it's conceivable that ATP binding and substrate binding (through the induced-fit process) block the gates/portals to the drug-binding pocket, whereas ATP hydrolysis rearranges the TM segments, allowing drug substrate to be released from P-gp.

1.5 Changes in Conformation During the Transport Cycle

Drug efflux occurs when ATP interacts with NBDs, changing the drug-binding sites from a high-affinity to a low-affinity state. The release of drug substrate will necessitate conformational changes in the drug-binding pocket since the common drug-binding pocket is rather big and substrates bind via an induced-fit process. Spectroscopic and cryo-electron microscopy have revealed global alterations in P-gp structure in response to nucleotide binding[24].

Using cysteine-scanning mutagenesis and thiol-reactive chemicals, conformational alterations in the TM segments around the common drug-binding pocket have also been

[23] Rosenberg et al., "Three-Dimensional Structures of the Mammalian Multidrug Resistance P-Glycoprotein Demonstrate Major Conformational Changes in the Transmembrane Domains upon Nucleotide Binding *."
[24] Rosenberg et al.

observed. Because both TMs contribute residues to the drug-binding pocket, early research on conformational changes in P-gp focused on TM 6 and TM12. Disulfide cross-linking between cysteines inserted at the extracellular ends of these TMs was used to identify conformational changes between TM6 and TM12 during ATP hydrolysis (residue L332C in TM6 and L975C in TM12). Cross-linking between L332C and L975C inhibited ATPase function by preventing conformational changes during ATP hydrolysis. When the disulfide link was broken with the reducing agent dithiothreitol, the activity was restored. A monoclonal antibody was used to identify TM12 involvement in conformational changes. After trapping intermediates using the cross-linker substrate Tris-(2-maleimidoethyl)amine (TMEA), it was discovered that ATP hydrolysis pushed TM6 away from TM12.

TMEA was used to cross-link a cysteine in TM12 (Cys982) to a cysteine in TM6 (Cys339) in this work. Cys982(TM12) may now be cross-linked to Cys343 in the presence of ATP (TM6). When the residues in TM6 and TM12 are organized in -helical wheels, they show that ATP hydrolysis caused TM6 to spin and/or shift laterally in relation to TM12[25]. The possibility of hydration of the drug substrate is another reason why ATP hydrolysis might lead to drug release. The drug substrate is thought to get dehydrated as it enters the lipid bilayer. Before being released into the extracellular media, the drug substrate diffuses into the common drug-binding pocket, where it can be rehydrated.

During ATP hydrolysis, the labeling of residues in the drug-binding pocket with the hydrophilic chemical MTSES was increased (Loo et al., 2004b). This data showed that during ATP hydrolysis, the drug-binding pocket becomes more accessible to water. Rehydration of the substrate is a crucial stage in the transport cycle because it prevents the substrate from diffusing

[25] Loo, Bartlett, and Clarke, "Disulfide Cross-Linking Analysis Shows That Transmembrane Segments 5 and 8 of Human P-Glycoprotein Are Close Together on the Cytoplasmic Side of the Membrane."

back into the lipid bilayer and prepares it for release into an aqueous environment[26]. Another question about P-gp function is whether drug substrates are transported directly out of the lipid bilayer or whether P-gp simply serves as a flippase to transport the substrate from the inner leaflet to the outside leaflet of the bilayer.

1.6 Anaplastic lymphoma kinase(ALK) inhibitors

For ALK-rearranged NSCLC patients, treatment with ALK-TKIs, such as Crizotinib, Ceritinib, or Alectinib often leads to conspicuous tumor shrinkage; however, tumors inevitably relapse because of acquired resistance approximately within 1–2 years of treatment. The chromosomal rearrangement-induced anaplastic lymphoma kinase (ALK) fusion oncogene has been found in a number of human cancers, including ALK-rearranged non-small cell lung cancer (NSCLC), which was discovered in 2007[27]. A chromosomal inversion event causes fusion of a part of the ALK gene with the echinoderm microtubule–associated protein–like 4 (EML4) gene in a small proportion of NSCLC cancers. The EML4-ALK fusion protein that results is permanently active and transformative, resulting in oncogene addiction. EML4-ALK fusion and other ALK rearrangements are seen in 3–7% of individuals with NSCLC also known as "ALK-positive" lung cancer and are linked to younger age, never or mild smoking history, and adenocarcinoma histology. [28]

Patients with advanced ALK-positive NSCLC respond well to the ALK inhibitor crizotinib (Xalkori, Pfizer), with a 60 percent objective response rate (ORR) and a median progression-free survival (PFS) of 8 to 10 months[29]. However, the advent of drug resistance has dampened enthusiasm for crizotinib. Most ALK-positive lung cancer patients who respond to

[26] Loo, Bartlett, and Clarke.
[27] Du et al., "ALK-rearrangement in Non-small-cell Lung Cancer (NSCLC)."
[28] Du et al.; Du et al.
[29] Shaw et al., "Crizotinib versus Chemotherapy in Advanced ALK-Positive Lung Cancer."

crizotinib experience a recurrence within a few years after commencing treatment[30]. In patients with ALK-positive NSCLC, the central nervous system (CNS) is one of the most prevalent sites of recurrence, and CNS illness might be resistant to conventional treatments[31].

Table 1
Characteristics of ALK Inhibitors

Drug	Pharmaceutical company	Maximum Dose	Targets other than ALK	Toxicities
Ceritinib (Zykadia)	Pfizer	750 mg daily	IGF-1R INSR STK22D	Diarrhea, vomiting, nausea, dehydration, ALT elevation, and hypophosphatemia are all symptoms of a bacterial infection.
Crizotinib (Xalkori)	Novartis	250 mg twice daily	c-MET ROS1	Diarrhea, nausea, vomiting, constipation, aminotransferase increase, edema, upper respiratory infection, dysgeusia, and dizziness are among symptoms that might occur.
Alectinib (Alecensa)	Roche	300 mg twice daily	LTK GAK	Dysgeusia, abnormal liver function tests, elevated serum creatinine, rash, gastrointestinal side effects, reduced neutrophil count, elevated serum creatine phosphokinase, stomatitis, and myalgias are all possible adverse effects.

Note: Adapted from Awad, M. M., & Shaw, A. T. (2014, July). *ALK inhibitors in non-small cell lung cancer: Crizotinib and beyond*. Clinical advances in hematology & oncology

1.7 Ceritinib (Zykadia) and it's pharmacokinetics

Ceritinib (Zykadia, Novartis; formerly known as LDK378) is a strong ALK inhibitor that was authorized by the FDA in 2017 and is developed from Novartis' lead chemical TAE684. In ALK enzymatic tests, it has an IC50 of 200 pM, while in cell-based assays, it has an IC_{50} of around 25 nM. The daily treatment of ceritinib to rat xenograft models using the H2228 NSCLC EML4-ALK cell line resulted in full tumor shrinkage. Ceritinib significantly inhibited ALK with

[30] Shaw et al.
[31] Otterson et al., "Clinical Characteristics of ALK+ NSCLC Patients (Pts) Treated with Crizotinib beyond Disease Progression (PD)."

the crizotinib-resistant mutations L1196M, G1269A, I1171T, and S1206Y in ALK-positive cell line models, but it was ineffective against ALK with the G1202R and F1174C mutations[32].

It has been found that the peak plasma levels of Ceritinib(Cmax) were reached in individuals after a single oral administration of ZYKADIA at around 4 to 6 hours, and the area under the curve(AUC) and Cmax increased dose proportionately over 50 to 750mg. This drug's absolute bioavailability has yet to be confirmed.

After three weeks of ZYKADIA 750 mg once daily dosing in human patients, steady-state was reached after around 15 days, with a geometric mean accumulation ratio of 6.2. Repeated dosages of 50 to 750 mg once daily enhanced systemic exposure in a dose-proportional way. Ceritinib's systemic exposure was raised when given with a meal. A food effect study in healthy subjects with a single 500 mg Ceritinib dose revealed that a high fat meal (containing approximately 1000 calories and 58 grams of fat) increased Ceritinib AUC by 73 percent and Cmax by 41 percent, while a low fat meal (containing approximately 330 calories and 9 grams of fat) increased Ceritinib AUC by 58 percent and Cmax by 43 percent. [33]

A ZYKADIA dose of 600 mg or more taken with a meal is predicted to result in systemic exposure greater than a 750 mg ZYKADIA dose given fasting, thereby increasing adverse drug responses[34]. Ceritinib binds to human plasma proteins 97 percent of the time, regardless of medication concentration, it also exhibits a minor preference for red blood cells in comparison to plasma, with a mean blood to plasma ratio of 1.35 in vitro. In vitro experiments also revealed that CYP3A was the primary enzyme involved in Ceritinib metabolic clearance.

[32] Friboulet et al., "The ALK Inhibitor Ceritinib Overcomes Crizotinib Resistance in Non–Small Cell Lung Cancer."
[33] "205755lbl.Pdf."
[34] "205755lbl.Pdf."

Ceritinib, the parent molecule, was the major circulating component in human plasma (82 percent) following oral administration of a single 750 mg radiolabeled Ceritinib dosage. 92.3 percent of a single 750 mg radiolabeled Ceritinib dose was recovered in the feces with 68 percent as unmodified parent component, while 1.3 percent was recovered in the urine after oral delivery. Ceritinib is a potent inhibitor of CYP3A and a mild inhibitor of CYP2C9[35]. In 19 healthy adults, coadministration of a single 450 mg ZYKADIA dosage with 200 mg ketoconazole (a potent CYP3A inhibitor) twice daily for 14 days elevated ceritinib AUC (90 percent CI) by 2.9-fold (2.5, 3.3) and Cmax (90 percent CI) by 22% (7%, 39%). Ceritinib is a substrate of the efflux transporter P-gp in vitro, but not of the Breast Cancer Resistance Protein (BCRP), Multidrug Resistance Protein (MRP2), Organic Cation Transporter (OCT1), Organic Anion Transporter (OAT2), or Organic Anion Transporting Polypeptide (OATP1B1). Ceritinib concentrations may be increased by drugs that inhibit P-gp[36].

1.8 Crizotinib(Xalkori) and it's pharmacokinetics

Crizotinib is a tyrosine kinase inhibitor that targets ALK, Hepatocyte Growth Factor Receptor (HGFR, c-Met), ROS1 (c-ros), and Recepteur d'Origine Nantais (RON). Translocations can alter the ALK gene, causing oncogenic fusion proteins to be expressed. The creation of ALK fusion proteins causes the gene's expression and signaling to be activated and dysregulated, which can lead to enhanced cell proliferation and survival in tumors expressing these proteins.

Crizotinib inhibited ALK, ROS1, and c-Met phosphorylation in tumor cell lines and showed anticancer efficacy in mice harboring tumor xenografts expressing echinoderm microtubule-associated protein-like 4 (EML4)- or nucleophosmin (NPM)-ALK fusion proteins or c-Met in cell-based tests. With a median accumulation ratio of 4.8 after using XALKORI 250

[35] Hurtado et al., "Effect of Ceritinib on the Pharmacokinetics of Coadministered CYP3A and 2C9 Substrates."
[36] "205755lbl.Pdf."

mg twice daily for 15 days, steady-state was attained and remained constant. Over the dose range of 200 mg to 300 mg twice day (0.8 to 1.2 times the authorized recommended dosage), the steady-state observed minimum concentration (Cmin) and AUC rose in a more than dose-proportional way.

The median duration to reach peak concentration after a single crizotinib dosage was 4 to 6 hours, and the mean absolute bioavailability of crizotinib was 43%. (range: 32 percent to 66 percent). crizotinib is metabolized mostly by CYP3A. Following a single oral 250 mg dosage of radiolabeled crizotinib, 63 percent (53 percent as unaltered) of the given dose was recovered in feces and 22 percent (2.3 percent as unchanged) in urine in healthy participants[37].

In comparison to crizotinib alone, coadministration of a single 150 mg oral dosage of crizotinib with ketoconazole, a potent CYP3A inhibitor, raised crizotinib AUC0-INF by 216 percent and Cmax by 44 percent. In comparison to crizotinib alone, coadministration of XALKORI 250 mg orally once daily with itraconazole, a potent CYP3A inhibitor, raised crizotinib steady-state AUC by 57% and Cmax by 33%. It was also found that P-gp, organic cation transporter (OCT) 1, and OCT2 are all inhibited by crizotinib. It had no effect on the organic anion transporting polypeptides (OATP) B1, OATP1B3, organic anion transporter (OAT) 1, OAT3, or the bile salt export pump transporter (BSEPT) (BSEP)[38].

1.9 Pharmacokinetics of Alectinib(Alecensa)

Alectinib is a tyrosine kinase inhibitor that inhibits the ALK and RET pathways. In nonclinical studies, alectinib reduced tumor cell viability in multiple cell lines with ALK fusions, amplifications, or activating mutations by inhibiting ALK phosphorylation and ALK-mediated

[37] "202570s030lbl.Pdf."
[38] "202570s030lbl.Pdf."

activation of the downstream signaling proteins STAT3 and AKT, and inhibiting ALK-mediated activation of the downstream signaling proteins STAT3 and AKT.

Alectinib has been shown to be effective against the crizotinib-resistant ALK mutations L1196M, C1156Y, and F1174L in preclinical studies, suggesting that it may be useful in patients who have developed crizotinib resistance through these pathways. Alectinib inhibits the activating mutations F1174L and R1275Q, which are present in neuroblastoma, indicating a possible therapeutic application for this drug in neuroblastoma[39].

M4, alectinib's main active metabolite, exhibited similar potency and activity in vitro. Administration of alectinib to mice implanted with tumors containing ALK fusions resulted in anticancer activity and extended life, even in mice implanted intracranially with ALK-driven tumor cell lines. CYP3A4 converts alectinib to its main active metabolite M4. At steady-state, the geometric mean metabolite/parent exposure ratio is 0.40. M4 is then metabolized by the enzyme CYP3A4. The major circulating compounds in plasma were alectinib and M4, accounting for 76 percent of the total radioactivity.

Following oral administration of a single radiolabeled dosage of alectinib in fed circumstances, 98% of the radioactivity was excreted in stool. Eighty-four percent of the dosage was excreted unaltered as alectinib in the stool, and six percent was excreted as M4. The amount of radioactivity excreted in urine was less than 0.5 percent of the radiolabeled dosage of alectinib given. There were in vitro studies that show that alectinib and M4 do not appear to inhibit CYP1A2, 2B6, 2C9, 2C19, or 2D6 in vitro[40]. The goal of this paper is to determine a comprehensive model describing the molecular mechanism of triptan transport by Pgp. It was done by testing the molecular interactions of ceritinib, crizotinib and alectinib with the

[39] Sakamoto et al., "CH5424802, a Selective ALK Inhibitor Capable of Blocking the Resistant Gatekeeper Mutant."
[40] "208434s001lbl.Pdf."

transporter. Testing the effect that these ALK inhibitors have on Pgp coupled ATP hydrolysis. The interactions were also tested by using protein fluorescence spectroscopy using the tryptophan quenching and acrylamide quenching methods.

CHAPTER 2

MATERIALS AND METHODS

2.1 Materials

Ceritinib, Crizotinib and Alectinib was purchased from Sigma-Alrich. Alfa Aesar provided digoxin, ethylene glycol tetraacetic acid (EGTA), and imidazole. EMD Millipore Corporation provided the n-dodecyl—D-maltoside (DDM) detergent used in protein purification. Avanti Polar Lipids Inc provided Escherichia coli complete lipid extract powder. Gold Biotechnology was the source of DTT. Acrylamide was purchased from milliporesigma and sodium orthovandate was purchased from Enzo Life Sciences.

2.2 Expression and purification of the mouse Pgp transporter

Using nickel-nitrilotriacetic acid (Ni-NTA) (Thermo Fisher Scientific) and diethylaminoethyl cellulose (DEAE) resin, the his-tagged wild type mouse Pgp (Abcb1a, MDR3) was isolated from Pichia (P.) pastoris (Thermo Fisher Scientific)[41]. The yeast cells were cultivated and induced with methanol in a 32 l DCI-Biolafitte fermenter with a 20 l working capacity at the University of Georgia's Bioexpression and Fermentation Facility, following a similar method as previously described[42]. Rather than utilizing glass bead breaking or the French press to fracture the yeast cells, the cells were broken by liquid nitrogen freezing and mixing for a minimum of six passes. After the nickel-nitrilotriacetic acid (Ni-NTA) column stage, no further DDM was added to lower the quantity of DDM in our activity tests and during liposome production. Typically protein purification yields from previous lab members yields for 100g of

[41] "A Gene Optimization Strategy That Enhances Production of Fully Functional P-Glycoprotein in Pichia Pastoris."
[42] Nandigama et al., "Large-Scale Purification of Functional Human P-Glycoprotein (ABCB1)."

wet weight cells were 122mg, which is comparable to earlier yields[43]. The protein was found to be >95 percent pure after SDS/PAGE screening. Using Amicon Ultra-15 100 kDa cut-off filters (EMD Millipore, Billerica, MA), the protein was concentrated to 150 M and kept at 80°C in 10 mM Tris/HCl, 30% glycerol with a pH of 8.0.

2.3 Integration of P-glycoprotein(Pgp) into liposomes

Using the filter extrusion technique, Pgp was reconstituted into 400 nm unilamellar liposomes.The liposomes were made out of 20% w/v cholesterol and 80% w/v Avanti E. coli Total Lipid Extract (Avanti Polar Lipids) with a specified lipid profile. In chloroform, lipids and cholesterol were combined to a final volume and concentration of 10 ml and 10 mgml1, respectively[44]. The liposomes were made out of 20% w/v cholesterol and 80% w/v Avanti E. coli Total Lipid Extract (Avanti Polar Lipids) with a specified lipid profile. In chloroform, lipids and cholesterol were combined to a final volume and concentration of 10 ml and 10 mgml, respectively. In a Buchi Rotavapor Model R-114, this organic solution was evaporated to dryness (Buchi). This was resuspended in 10 ml of 50 mM Tris/HCl and 0.1 mM EGTA (pH 7.4). Liquid nitrogen was used to freeze and thaw the suspension at least ten times. The rehydrated lipid was extruded 11 times with a Millipore 400 nm cutoff filter using a LIPEX extruder (Northern Lipids) (EMD Millipore). To remove leftover detergent, 100 M of Pgp was dialyzed for 2 hours in HEPES buffer that contained 20 mM HEPES, 100 mM sodium chloride, 5 mM magnesium chloride, 2 mM DTT in a pH of 7.4. Then, for 1 hour, 50 M of dialyzed protein and 4 mgml1 liposomes were incubated. This was then dialyzed against HEPES buffer for another 2 hours to enhance protein integration into the liposomes. The reconstituted liposomes were spun for 5

[43] "A Gene Optimization Strategy That Enhances Production of Fully Functional P-Glycoprotein in Pichia Pastoris."
[44] Chifflet et al., "A Method for the Determination of Inorganic Phosphate in the Presence of Labile Organic Phosphate and High Concentrations of Protein."

minutes at 100 g in a Sorvall Legend Micro 21 centrifuge to remove aggregated Pgp (ThermoScientific).

2.4 ATPase activity measurements

The Chifflet technique was used to determine the Pgp transporter's ATPase activity[45]. The technique measures the concentration of free Pi following ATP hydrolysis by the production of a Pi–molybdenum complex, which generates a high absorbance signal at 850 nm, which is used to assess ATPase activity. In a FlexStation 3 spectrometer, the absorbance at 850 nm was measured on a 96-well plate (Molecular Devices). With 50 nM Pgp in Chifflet buffer that included 150 mM ammonium chloride, 5 mM magnesium sulfate, 0.02 percent w/v sodium azide, 50 mM Tris/HCl, 2 mM DTT in a pH of 7.4. The ATPase activity of ceritnib, crizotinib and alectinib was evaluated.

Nonlinear regression was used to model the Pgp-mediated ATP hydrolysis kinetics using the Igor Pro 6.2 software (Wavemetrics, Tigard, OK). The modified Michaelis-Menten equation, where v is the ATP hydrolysis rate, V_{sat} is the maximum ATP hydrolysis rate at saturating drug, [L] is the ligand concentration, K_m is the Michaelis-Menten constant, and V_{basal} is the basal ATPase activity in the absence of the drug, was used to fit monophasic ATPase kinetics curves.

$$v = \frac{V_{MAX}[L]}{K_m + [L]} + v_{basal}$$

Equation 1

[45] Chifflet et al.

2.5 Pgp affinity measurements by fluorescence quenching

The dissociation constants of Pgp and different ligands have been measured by quenching intrinsic protein fluorescence. This method was used to determine the binding affinity of Pgp to anthracycline medicines. Using an Olis DM 45 spectrofluorimeter (Olis Corporation, Bogart, GA), protein fluorescence emission was measured between 300 and 500 nm, with an emission maximum at about 330 nm following excitation at 295 nm. To avoid protein aggregation, proteoliposome samples for fluorescence studies contained 1 mM Pgp and 100 mM potassium phosphate buffer with 2 mM DTT[46]. Background, volume, and inner filter effects were all taken into account when the medicines quenched Pgp's fluorescence. F represents the observed protein fluorescence at 330 nm, B is the background, [Q] is the ligand concentration, and ε_{ex}, ε_{em}, b_{ex} and b_{em} are the excitation and emission extinction coefficients and pathlengths, respectively.

$$F_{corrected} = (F - B)10^{\frac{\varepsilon_{ex} b_{ex} + \varepsilon_{em} b_{em}[Q]}{2}}$$

Equation 2

Static quenching refers to drug-induced quenching of protein fluorescence caused by ligand complexation with the protein, which may be used to measure the drug's affinity. Dynamic quenching is the term for drug-induced fluorescence quenching caused by random protein collisions. The fluorescence quenching curves were fitted to equation 3 regardless of the nature of the quenching. $F_{corrected,0}$ represents the fluorescence of the protein with no quenching

[46] Wilt, Nguyen, and Roberts, "Insights into the Molecular Mechanism of Triptan Transport by P-Glycoprotein."

ligand present and K is the association constant(K_A) or the stern volmer quenching constant (K_{SV}) in the situation of static and dynamic quenching processes.

$$F_{\text{corrected}} = \frac{F_{\text{corrected},0}}{1 + K\,[Q]}$$

Equation 3

By measuring the protein's fluorescence life time in the presence of the quenching ligand or doing fluorescence titration studies at two different temperatures, the two distinct quenching processes may be distinguished[47]. In the latter instance, the K increases with rising temperature for dynamic quenching by raising the quencher's collisional frequency and decreases with increasing temperature for static quenching by lowering the quenching ligand's residence time[48].

Acrylamide is known as a quencher that has been used to investigate the accessibility of tryptophans in proteins as well as changes in the quenching ligand's tertiary structure. Pgp structural changes were investigated using dynamic quenching of intrinsic tryptophan fluorescence by acrylamide. Fluorescence emission with Pgp that was integrated into liposomes was measured at 333 nm after excitation at 295 nm for these studies. To evaluate the degree of non-specific quenching, control acrylamide titrations were performed in the presence of N-acetyl-L-tryptophanamide (NATA). Equation 2 was used to adjust for fluorescence intensity, the $F_{corrected},0/F_{corrected}$ ratio was displayed as a function of acrylamide concentration to create the Stern–Volmer plots. The slopes of the Stern–Volmer curves, which are linked to KSV by

[47] "Unravelling the Complex Drug–Drug Interactions of the Cardiovascular Drugs, Verapamil and Digoxin, with P-Glycoprotein | Bioscience Reports | Portland Press."
[48] Lakowicz, "Mechanisms and Dynamics of Fluorescence Quenching."

$F_{corrected},0/F_{corrected}$= 1 + KSV[Q], were used to assess the degree of dynamic tryptophan quenching.

The extinction coefficient at 295nm for alectinib was 1.65$mM^{-1}cm^{-1}$ and 0.95$mM^{-1}cm^{-1}$ at 330nm. The extinction coefficient at 295nm and 330nm for ceritinib was 0.56$mM^{-1}cm^{-1}$ and 0.69$mM^{-1}cm^{-1}$. The extinction coefficient at 295nm for crizotinib was 0.30$mM^{-1}cm^{-1}$ and 0.54$mM^{-1}cm^{-1}$ at 330nm. The extinction coefficient of P-glycoprotein at 295nm was found to be 0.092$\mu M^{-1}cm^{-1}$ and was transparent at 330nm.

CHAPTER 3

RESULTS

The primary focus on this section is to discuss the method development process and the results of the analysis performed to determine the transport rate, binding affinity and P-gp conformational changes with ALK- inhibitors.

3.1 The effect of Certinib, Crizotinib and Alectinib on the Pgp-coupled ATPase activity

ATP consumption indicates ATPase activity because ABC transporters employ energy generated by ATP hydrolysis to pump their substrate agents out of MDR cells against a concentration gradient. To learn more about how the following ceritinib, crizotinib and alectinib inhibits ABCB1 function, ATPase activity in the presence of various drug doses was tested.

This study shown below demonstrates the effect of the following ALK inhibitors ceritinib, crizotinib and alectinib on Pgp-mediated activity in the presence of 13mM ATP. In Figure 3.1 the curves present were fit to Equation 1 to determine the ATPase velocity with saturating drug and the K_m values. Figure 3.1A shows ATP hydrolysis with ceritinib that resulted in a K_m value of $3.9 \pm 0.6 \mu M$ and a V_{max} value of 135 ± 5.11nmol min^{-1} mg^{-1}. The ATPase activity was stimulated by ceritinib until it reached a plateau near 380nmol min^{-1} mg^{-1}. Figure 3.1B shows ATP hydrolysis with crizotinib that resulted in a K_m value of $12.3 \pm 3.5 \mu M$ and a V_{max} value of 282.184 ± 10nmol min^{-1} mg^{-1}. The ATPase activity was stimulated by crizotinib until it reached a plateau near 400nmol min^{-1} mg^{-1}.

Figure 3.1C shows ATP hydrolysis with alectinib that resulted in a lower K_m and V_{max} value of $0.8 \pm 0.02 \mu M$ and 179.48 ± 8.03nmol min^{-1} mg^{-1} compared to ceritinib and crizotinib.

The ATPase activity was stimulated by alectinib until it reached a plateau near 43nmol min^{-1} mg^{-1}.

Figure 3.1D represents ATP hydrolysis with verapamil which is a calcium-channel blocker and is known as a strong inhibitor of Pgp and it has been used as a control to assess the ATPase activity of the anticancer drugs in this study. This resulted in a biphasic kinetics of Pgp-coupled ATP hydrolysis with a K_m value of $1.96 \pm 8.02 \mu M$, Ki value of $497 \pm 43 \mu M$ and a Vmax value of 11439 ± 2.42nmol min^{-1} mg^{-1}. Ceritinib, crizotinib and alectinib was shown to boost ATPase activity in the same way that other substrates did by engaging with the drug-substrate-binding sites on the transporters. Ceritinib however showed the least K_m value demonstrating it has a higher transport rate.

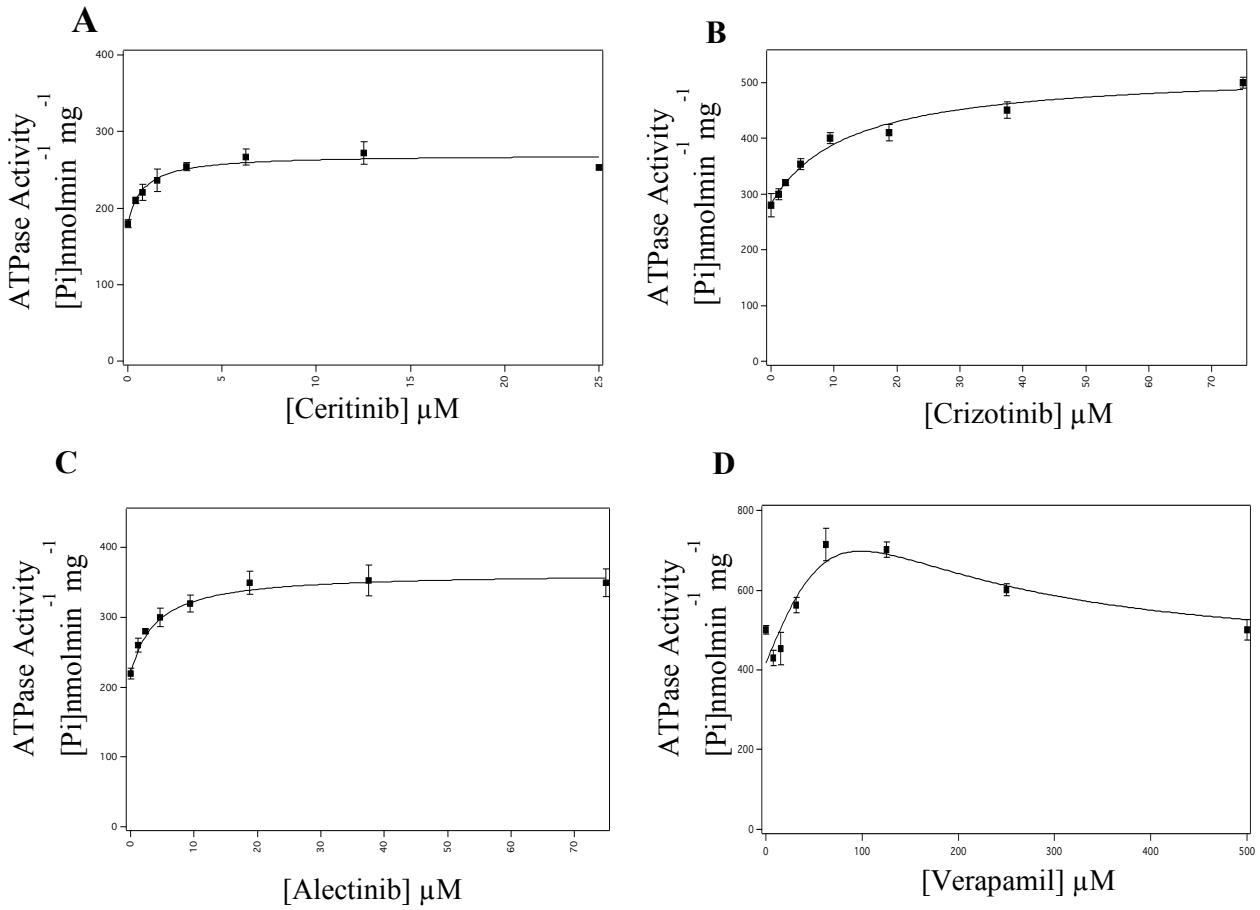

Figure 3.1 ATPase activity in response to different concentrations of (A)15mM Ceritinib, (B) 15mM Crizotinib and (C) Alectinib showing the effects of it on P-gp mediated ATP hydrolysis. (D) represents the ATPase activity as a control in response to different concentrations of verapamil. The error bars indicate the standard deviation, while the dots represent the average of at least three studies. Solid lines represent fits to the locations using equation 1 that was demonstrated earlier.

3.2 Determining the affinity of ceritinib, crizotinib and alectinib with Pgp determined by intrinsic protein fluorescence quenching

The binding affinities of ceritinib, crizotinib and alectinib were estimated through intrinsic tryptophan quenching of P-gp protein fluorescence and is shown in the figure below. When the protein was stimulated between 280, inner filter effects and background fluorescence by the three anticancer drugs significantly obscured Pgp fluorescence at 333 nm. The detrimental effects of the ALK inhibitors on the protein fluorescence signal were reduced when the protein was excited at 295 nm.

Figure 3.2A, 3.2B and 3.2C shows the Pgp fluorescence in the presence of a range of ceritinib, crizotinib and alectinib concentrations were monitored at 333nm and adjusted for inner filter effects using equation 2. When Pgp was stimulated at 295 nm, it was most susceptible to drug-induced protein fluorescence quenching.

Fitting the protein fluorescence quenching curve in figure 3.2A with equation 3 the $F_{corrected}$ at 333nm was plotted as a function of protein concentration and the addition of concentrations of ceritinib to a solution of a buffer with P-gp resulted in a slope of the stern-volmer plot resulted in a K_{SV} value of $0.62\pm0.0\ \mu M^{-1}$ and a K_D value of $5.95\pm0.5\mu M$. Crizotinib was measured with similar concentrations and in figure 3B with the $F_{corrected}$ was plotted at 333nm as a function of protein concentration resulted in a higher K_D value of $12.10\pm1.6\mu M$ and a K_{SV} value of $0.87\pm1.6\mu M^{-1}$. A K_{SV} value of $0.98\pm2.3\mu M^{-1}$ was extracted from fitting the protein fluorescence quenching curve in figure 3C with equation 3 the $F_{corrected}$ at 333nm was plotted as a function of protein concentration and the addition of concentrations of alectinib however resulted in a lower K_D value of $4.58\pm0.5\mu M$ that is similar to ceritinib. Comparing the three ALK inhibitors, crizotinib demonstrated the highest K_D value than both alectinib and ceritinib showing a higher binding affinity.

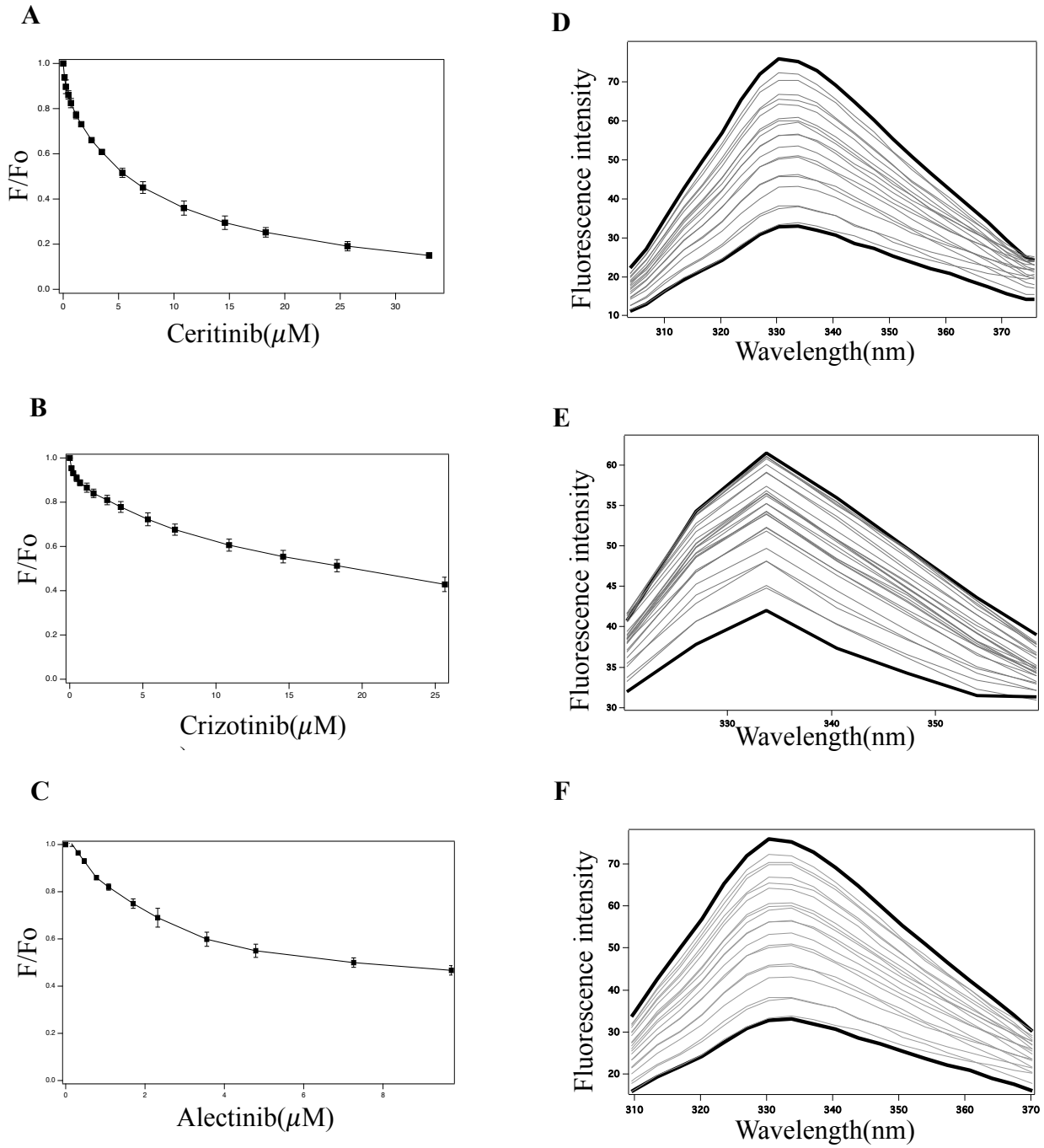

Figure 3.2 After correcting for inner filter effects with Equation 2, the fluorescence at 333 nm with a range of (A) 15mM ceritinib, (B) 15mM crizotinib and (C) 5mM alectinib concentrations. The error bars indicate the standard deviation, whereas the data points represent the average of at least three studies. Equation 3 fits to the points are given as solid lines. Pgp fluorescence emission spectra in the presence of a range of (D) ceritinib, (E) crizotinib and (F) alectinib concentrations following excitation at 295 nm. Pgp fluorescence is represented as thin and thick black lines in the absence and presence of saturating drug, respectively, whereas Pgp fluorescence with intermediate drug concentrations is displayed as gray lines.

3.3 Determining the affinity of ceritinib, crizotinib and alectinib with Pgp determined by intrinsic protein fluorescence quenching with AMP-PNP

Figure 3.3A, 3.3B and 3.3C shows the Pgp fluorescence in the presence of a range of ceritinib, crizotinib and alectinib concentrations when the non-hydrolyzable ATP analog was present. It was monitored at 333nm and adjusted for inner filter effects using equation 2. When Pgp was stimulated at 295 nm, it was most susceptible to drug-induced protein fluorescence quenching.

Fitting the protein fluorescence quenching curve in figure 3.3A with equation 3 the $F_{corrected}$ at 333nm was plotted as a function of protein concentration and the addition of concentrations of ceritinib to a solution of a buffer with P-gp resulted in a slope of the stern-volmer plot resulted in a K_{SV} value of $0.7\pm0.06\ \mu M^{-1}$ and a lower K_D value of $2.62\pm0.41\mu M$ compared to ceritinib without AMP-PNP present(Figure 3.2A, $5.95\ \pm0.5\mu M$).

Crizotinib was measured with similar concentrations and in figure 3.3B with the $F_{corrected}$ was plotted at 333nm as a function of protein concentration resulted in a lower K_D value of $9.56\pm1.81\mu M$ and a K_{SV} value of $0.85\pm0.03\mu M^{-1}$ when compared to crizotinib without AMP-PNP present(Figure 3.2B, $12.10\pm1.6\mu M$).

A K_{SV} value of $0.86\pm0.01\mu M^{-1}$ was extracted from fitting the protein fluorescence quenching curve in figure 3.3C with equation 3 the $F_{corrected}$ at 333nm was plotted as a function of protein concentration and the addition of concentrations of alectinib however resulted in a lower K_D value of $2.84\pm0.34\mu M$ that is similar to the previous study of ceritinib without AMP-PNP(Figure 3.2C, $4.58\pm0.5\mu M$).

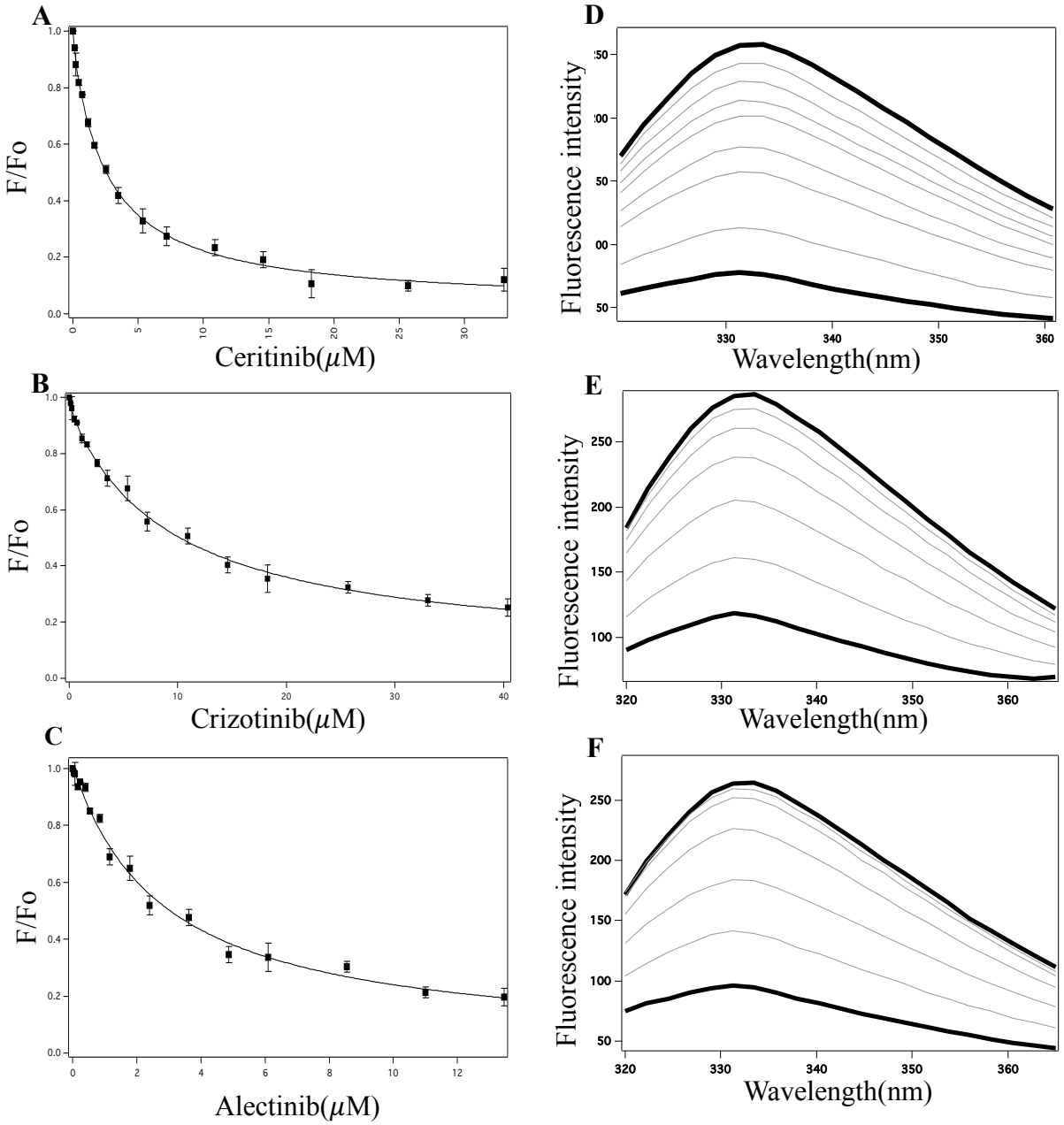

Figure 3.3 After correcting for inner filter effects with Equation 2, the fluorescence at 333 nm with a range of (A) 15mMceritinib with 3.2mM AMP-PNP(ATP analog) present, (B) 15mM crizotinib with presence of 3.2mM AMP-PNP(ATP analog) and (C)5mM alectinib in the presence of 3.2mM AMP-PNP(ATP analog) concentrations. The error bars indicate the standard deviation, whereas the data points represent the average of at least three studies. Equation 3 fits to the points are given as solid lines. Pgp fluorescence emission spectra in the presence of a range of (D) ceritinib, (E) crizotinib and (F) alectinib concentrations following excitation at 295 nm. Pgp fluorescence is represented as thin and thick black lines in the absence and presence of saturating drug, respectively, whereas Pgp fluorescence with intermediate drug concentrations is displayed as gray lines.

3.4 Pgp Conformational Changes in the presence of drugs as determined by Acrylamide Quenching

The drug-induced conformational changes of Pgp were investigated using acrylamide quenching of tryptophan fluorescence in the presence of the ALK inhibitors being studied including ceritnib, crizotinib and alectinib. The acrylamide quenching method makes use of the fact that tertiary conformational changes affect the solvent accessibility of fluorescent residues The effect of ceritnib, crizotinib and alectinib on the tertiary structure of Pgp was investigated using acrylamide quenching of protein fluorescence. When Pgp adopts a "open" conformation, fluorescent residues within the binding cavity are exposed to greater bulk solvent, resulting in a significant degree of acrylamide quenching however fluorescent residues inside the binding cavity are sequestered to bulk solvent when Pgp adopts a "closed" conformation, and acrylamide quenching is minimal. The slopes of Stern-Volmer plots were used to evaluate the relative degree of acrylamide quenching and the solvent accessibility of Pgp.

Figure 3.4 displays Stern–Volmer plots in the absence and presence of drugs to investigate protein structural changes and tryptophan accessibility. Figure 3.4A and 3.4B represent the controls used for the experiment to determine the degree of quenching in presence of 2M acrylamide for ceritinib, crizotinib and alectinib. In the absence of drugs(apoPgp), the slope of the Stern-Volmer plot for Pgp(Figure 3.4A, open circles) showed a K_{SV} value of $2\pm0.06M^{-1}$ whereas the Stern-Volmer plot for NATA(Figure 3.4A, dashed line) that was used to show the non-specific tryptophan interactions had a K_{SV} value of $15\pm0.2M^{-1}$ which represented the majority of Pgp's tryptophans that are out of reach to acrylamide. Figure 3.4B shows the Stern-Volmer plots apo-Pgp(open circles) and AMP-PNP(ATP analog adenylyl-

imidodiphosphate is present)(closed circles). The plot of Pgp in the presence of AMP-PNP resulted in a lower K_{SV} value than apoPgp of $1.3\pm0.05M^{-1}$.

Stern-Volmer plots of Pgp in the presence of increasing concentrations of ceritinib, crizotinib and alectinib are shown in Figures 3.4C, 3.4D and 3.4E. Figure 3.4C shows the plot of Pgp with low to high concentrations of ceritinib(closed triangles) resulting in a K_{SV} value of $4.2\pm2.3M^{-1}$ with respect to the controls of apoPgp(open circles) and AMP-PNP(closed circles). Figure 3.4D represents the Stern-Volmer plot of Pgp with increasing concentrations of crizotinib(closed squares) showed a relatively lower K_{SV} value to ceritinib which was $3.9\pm0.07M^{-1}$. Alectinib however resulted in a lower K_{SV} value than both ceritinib and crizotinib which was shown in figure 3.4E(closed circles) resulting in a K_{SV} value of $3.6\pm2.3M^{-1}$. These differences in K_{SV} values prove that there are conformational changes that occur to Pgp with the ligands present.

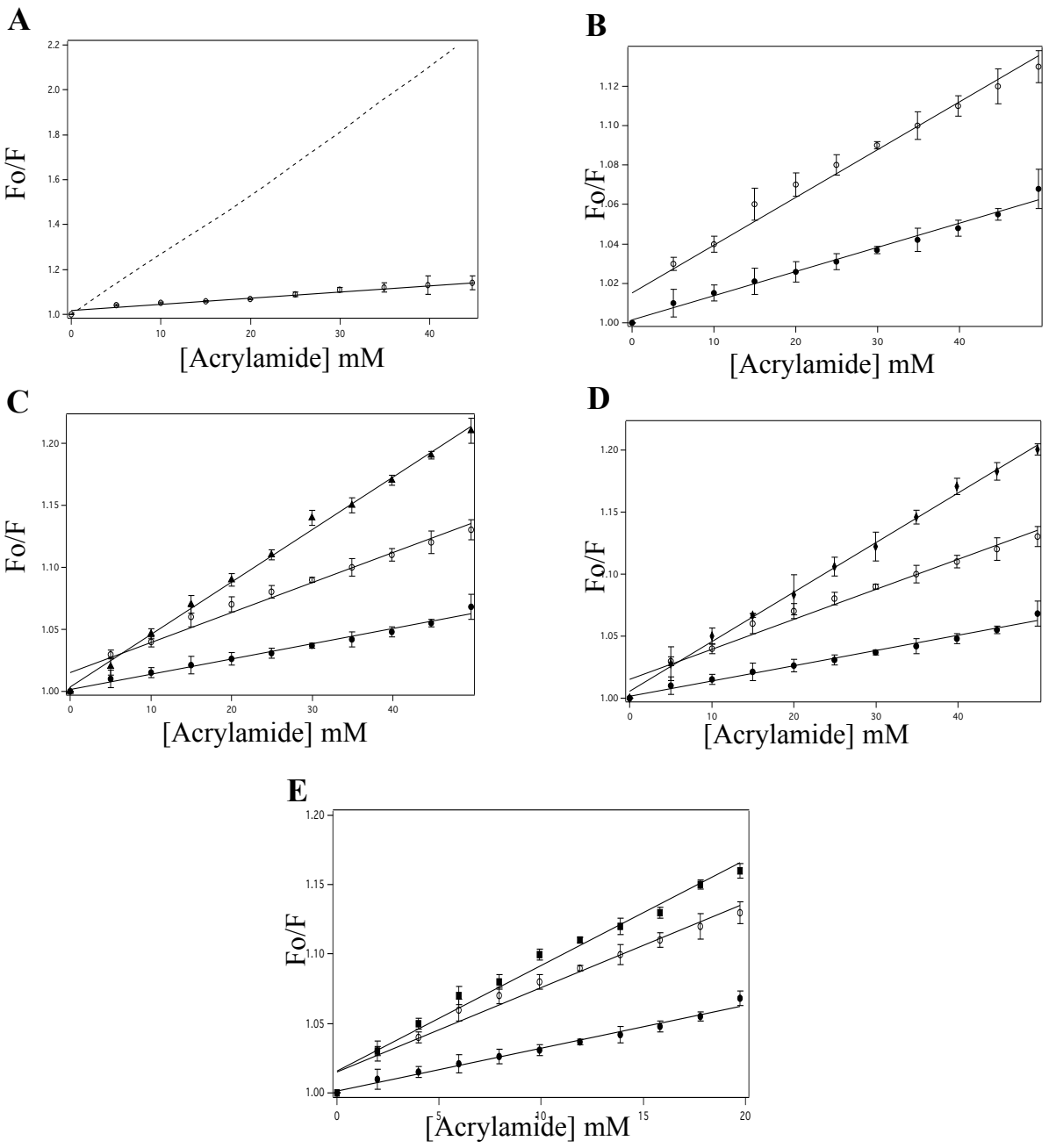

Figure 3.4 Acrylamide quenching of Pgp in the presence of ceritinib, crizotinib and alectinib. Figure 3.4A represents the stern volmer plot of NATA(dashed line) and Pgp with no drugs present representing closed configuration of Pgp (apoPgp, open circles) with increasing concentrations of acrylamide. Figure 3.4B shows apoPgp again(open circles) and pgp with 3.2mM AMP-PNP(represents open configuration of Pgp, open squares) with a range of acrylamide concentrations. Stern volmer plots of increasing concentrations of acrylamide with the addition of (C)15mM ceritinib(closed triangle), (D)15mM crizotinib(closed diamond) and (E) 5mM alectinib(closed square). The error bars indicate the standard deviation, while the data points represent the average of at least three studies. ApoPgp(open circles) and AMP-PNP(closed circles) were present in all plots (C), (D) and (E).

3.5 Pgp Conformational Changes in the presence of drugs as determined by Acrylamide Quenching with AMP-PNP

With a variety of ligands and nucleotide cofactors, acrylamide quenching of tryptophan fluorescence has been effectively utilized to investigate changes in Pgp's tertiary structure. This method was used to evaluate the influence of drug-nucleotide cooperativity on Pgp conformation in the presence of the ALK inhibitors and the non-hydrolyzable ATP analog AMP-PNP in this study. The ALK inhibitors in this study include certinib, crizotinib and alectinib.

Figure 3.5 depicts Stern-Volmer plots showing acrylamide quenching of Pgp with the ALK inhibitors and AMP-PNP, with the slopes representing the degree of tryptophan quenching. Figure 3.5A and 3.5B represent the same controls used for the experiment in Figure 3.4A, 3.4B to determine the degree of quenching in presence of 2M acrylamide for ceritinib, crizotinib and alectinib with AMP-PNP(ATP analog present). In the absence of drugs(apoPgp), the slope of the Stern-Volmer plot for Pgp(Figure 3.4A, open circles) showed a K_{SV} value of $2\pm0.06M^{-1}$ whereas the Stern-Volmer plot for NATA(Figure 3.4A, dashed line) that was used to show the non-specific tryptophan interactions had a K_{SV} value of $15\pm0.01M^{-1}$ which represented the majority of Pgp's tryptophans that are out of reach to acrylamide.

The experiment was tested with the same concentrations as previously shown in Figure 3.4. The Stern-Volmer plot for Pgp with ceritinib and AMP-PNP(Figure 3.5C,closed triangles) decreased the K_{SV} value by two folds from (Figure 3.4C, closed triangles) $4.2\pm2.3M^{-1}$ to $2.8\pm1.3M^{-1}$.

The Stern-Volmer plot for Pgp with increasing concentrations of crizotinib and AMP-PNP(Figure 3.5D, closed diamonds) showed to have little effect resulting in a K_{SV} value of $3.2\pm0.7M^{-1}$ when compared to $3.9\pm0.07M^{-1}$(Figure 3.4D, closed diamonds). A plot of Pgp with

alectinib and AMP-PNP(Figure 3.5E) on the other hand showed a decrease in the K_{SV} value from $3.6\pm2.3M^{-1}$ (Figure 3.4E, closed squares) to $1.96\pm0.7M^{-1}$.

Ceritinib and Alectinib showed significant shifts in the K_{SV} value in the presence of AMP-PNP(ATP analog) when compared to the Stern-Volmer plots in Figure 3.4 where the AMP-PNP(ATP analog) was not present.

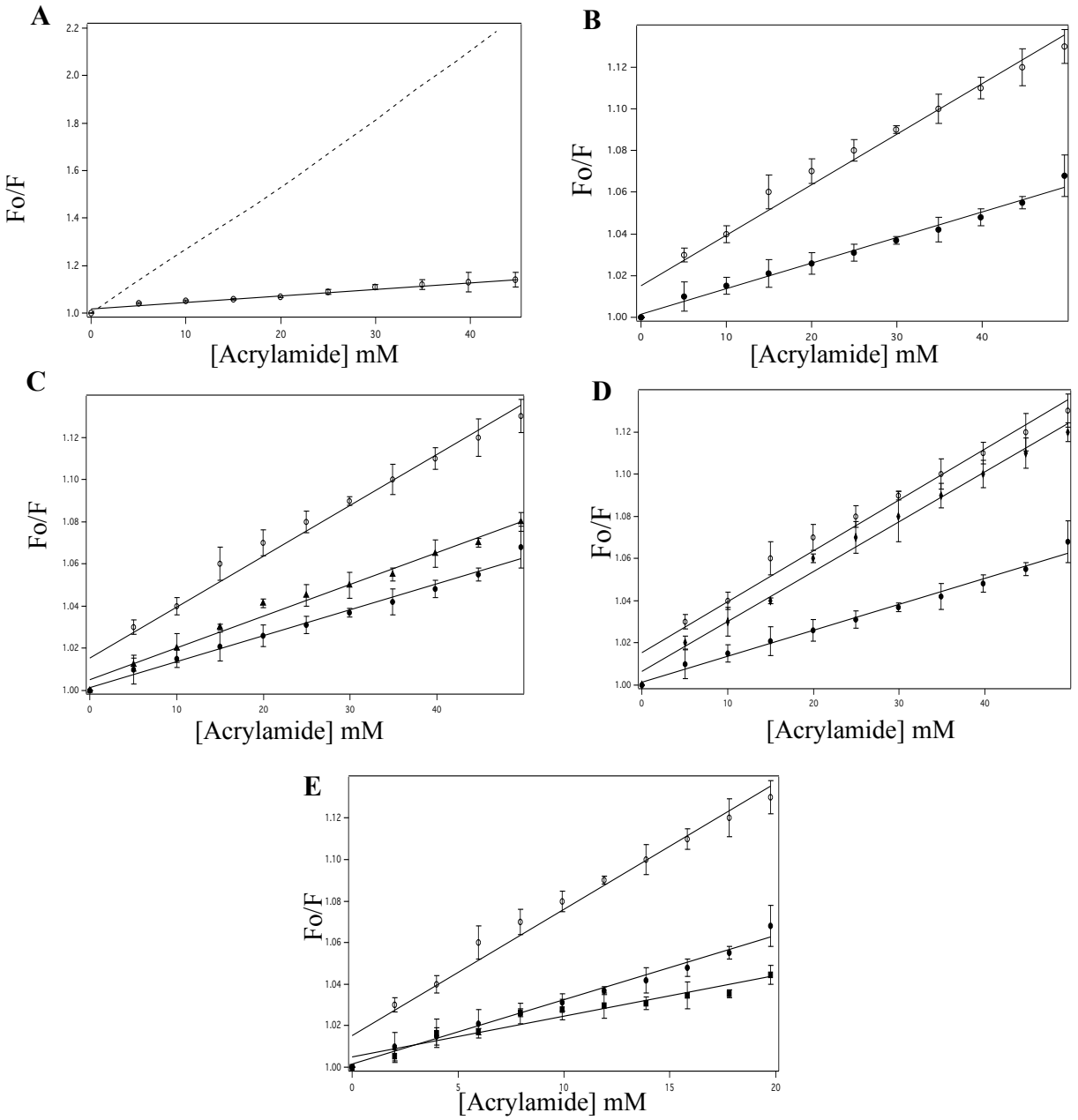

Figure 3.5 Acrylamide quenching of Pgp in the presence of AMP-PNP with ceritinib, crizotinib and alectinib . Figure 3.5A represents the stern volmer plot of NATA(dashed line) and Pgp with no drugs present representing closed configuration of Pgp (apoPgp, open circles) with increasing concentrations of acrylamide. Figure 3.5B shows apoPgp again(open circles) and pgp with 3.2mM AMP-PNP(represents open configuration of Pgp, open squares) with a range of acrylamide concentration. Stern volmer plots of increasing concentration of acrylamide with the addition of (C)15mM ceritinib with the presence of 3.2mM AMP-PNP(closed triangle), (D)15mM crizotinib in the presence of 3.2mM AMP-PNP(closed diamond) and (E) 5mM alectinib with 3.2mM AMP-PNP present(closed square). The error bars indicate the standard deviation, while the data points represent the average of at least three studies. ApoPgp(open circles) and AMP-PNP(closed circles) were present in all plots (C), (D) and (E).

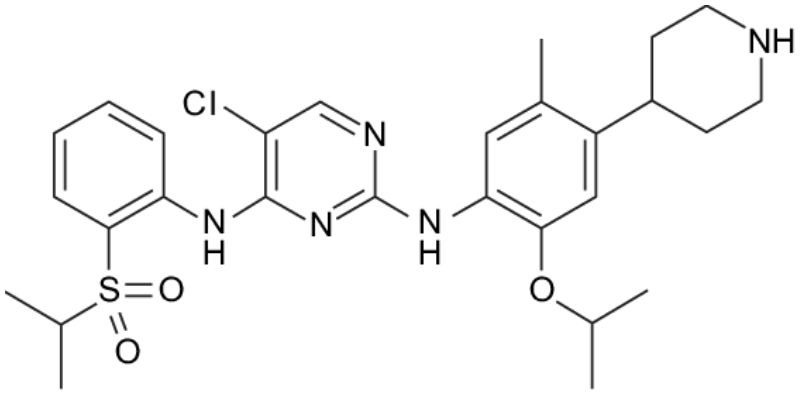

B

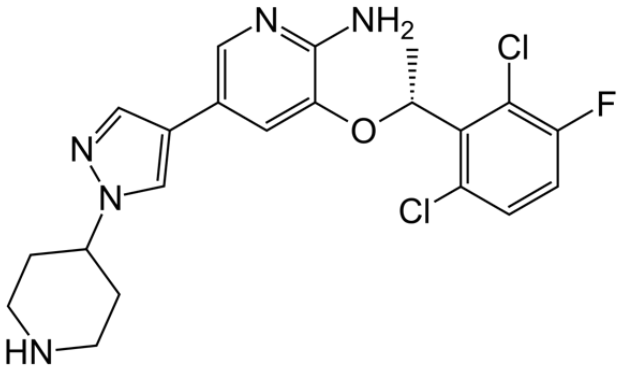

C

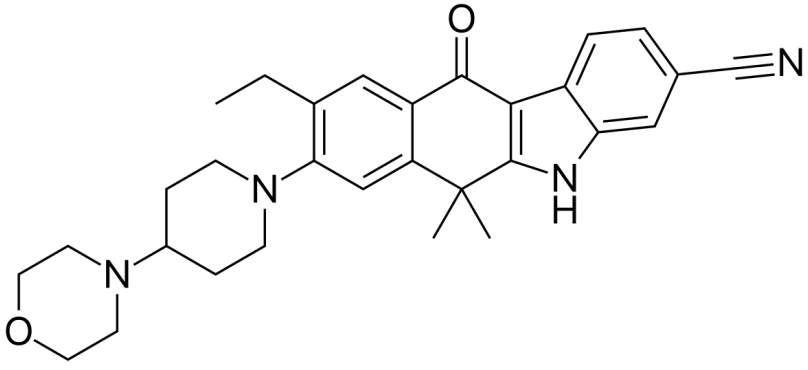

Figures 3.6 A, B and C represent the structures of ceritinib(A), crizotinib(B) and alectinib(C).

Table 2
Summary of results

	Ceritinib	Crizotinib	Alectinib
ATPase activity assay	K_m= $3.9\pm0.6\mu M$	K_m:$12.3\pm3.5\mu M$	K_m: $0.8\pm0.02\mu M$
	Vmax: 135 ± 5.11nmol min^{-1} mg^{-1}	Vmax: 282.184 ± 10nmol min^{-1} mg^{-1}	Vmax: 179.48 ± 8.03nmol min^{-1} mg^{-}
Tryptophan quenching	K_D: $5.95\pm0.5\mu M$	K_D: $12.10\pm1.6\mu M$	K_D: $4.58\pm0.5\mu M$
Tryptophan quenching with AMP-PNP	K_D: $2.62\pm0.41\mu M$.	K_D: $9.56\pm1.81\mu M$	K_D: $2.84\pm0.34\mu M$
Acrylamide quenching	Ksv: $4.2\pm2.3\mu M$.	Ksv: $3.9 \pm 0.07\mu M$.	Ksv: $3.6 \pm 2.3\mu M$
Acrylamide quenching with AMP-PNP	Ksv: $2.8\pm1.8\mu M$.	Ksv: $3.2 \pm 0.7\mu M$.	Ksv: $1.96 \pm 0.7\mu M$

CHAPTER 4

DISCUSSION

The mechanism behind Pgp-mediated drug transport is yet unknown. Models of transport have been developed in which substrates and ATP work together during transport. Other theories have been proposed in which substrates occupy various locations during efflux. Models of efflux transport have also been proposed, in which conformational changes cause efflux. Pgp conformations were previously simplified into a three-state model with "closed," "intermediate," and "open" conformations in earlier research with the transporter.

The NBDs are relatively widely apart in the 'open' conformation, and the cytosolic side is exposed to the bulk solvent. The NBDs are in touch with each other in the 'closed' conformation, and the extracellular side is exposed to the bulk solvent. Between the 'open' and 'closed' conformations lies the 'intermediate' conformation. P-gp's cytosolic and extracellular sides are accessible to the bulk solvent.

Cross-linking studies with Pgp, site-directed mutagenesis studies with Pgp, cryo-electron microscopy studies with Pgp, and structural studies with bacterial transporters with nucleotide analogs have all shown that the interaction of the P-gp nucleotide domains with each other is required for ATP hydrolysis.

The ATP hydrolysis rate was linked with the average distance between the P-gp NBDs in the model. Pgp with high and low ATP hydrolysis rates, for example, is believed to be in "closed" and "open" conformations, respectively. The degree of conformational shift was determined by measuring the ligand-induced changes in tryptophan accessibility of Pgp as determined by acrylamide quenching of tryptophan fluorescence.

ABCB1's drug efflux activity, like that of the other ABC transporters, is fueled by ATP hydrolysis. As a result, ATP consumption has been widely utilized to represent the transporter's ATPase activity. P-gp-mediated ATP hydrolysis was evaluated at different doses of crizotinib to determine the effect of ceritinib on the ATPase activity of P-gp. Ceritinib was discovered to be an activator of ABCB1 ATPase. Ceritinib enhanced ATPase activity in a dose-dependent manner, as demonstrated in Figure 3.1A as previously reported[49].

ABCB1 overexpression was thought to have a role in MDR by aggressively pumping its substrate anticancer medicines out of cells[50]. ABCB1 transport activity was investigated to learn more about the mechanism of ABCB1-mediated MDR reversal by crizotinib. Crizotinib was shown to dramatically enhance intracellular accumulation of doxorubicin and rhodamine 123 in ABCB1-overexpressing MDR cells in a dose-dependent manner while having no impact on the comparable parental KB and MCF-7 cells. Furthermore, crizotinb reduced drug efflux via ABCB1. As a result, crizotinib may be able to combat MDR by raising intracellular concentrations of its substrate anticancer medicines by inhibiting efflux as shown in previous studies where it is more likely known to be a substrate and a competitive inhibitor of P-gp[51]**.** With that being said this study proves that crizotinib stimulated ATPase activity in a dose-dependent manner, as demonstrated in Figure 3.1B.

Alectinib also demonstrated a activation of ATPase activity in increasing concentrations of alectinib which was evaluated in different doses of alectinib to determine its effect on the ATPase activity that was similar to previous studies[52]. Alectinib's activation of ABCB1 and

[49] Zhou et al., "Crizotinib (PF-02341066) Reverses Multidrug Resistance in Cancer Cells by Inhibiting the Function of P-Glycoprotein."
[50] Alexander, Mathie, and Peters, "Guide to Receptors and Channels (GRAC), 5th Edition."
[51] Alexander, Mathie, and Peters.
[52] Yang et al., "Alectinib (CH5424802) Antagonizes ABCB1- and ABCG2-Mediated Multidrug Resistance in Vitro, in Vivo and Ex Vivo."

ABCG2 ATPase activity at low doses implies that it is comparable to its substrates. Alectinib appears to be a competitive inhibitor of these transporters, in other words. Alectinib's interactions with ABCB1 and ABCG2 were further verified by its competition with the transporters' [125I]-IAAP photoaffinity labeling[53].

Tryptophan quenching of the ALK inhibitors without the presence of AMP-PNP in Figure 3.2 demonstrated that alectinib had the lowest K_D value followed by ceritinib whereas crizotinib had a much higher value of $12.10 \pm 1.6 \mu M$ (Figure 3.2B). Since both ceritinib and alectinib have a much lower K_D it could be assumed that they have a higher binding affinity drug transport when compared to crizotinib.

To explore nucleotide interactions with Pgp, the non-hydrolyzable ATP analog AMPPNP was utilized as a surrogate for ATP. Because it has been used to solve multiple comparable bacterial transporter X-ray crystal structures, the ATP analog is useful for studying nucleotide interactions with Pgp. In addition, unlike other nucleotide analogs, AMPPNP does not undergo ATP hydrolysis. Studies of tryptophan quenching with AMP-PNP showed to have a major effect where it caused the K_D values to decrease by at least two folds for ceritinib, crizotinib and alectinib.

The acrylamide quenching studies of Pgp with high and low concentrations of ceritinib, crizotinib and alectinib in Figure 3.4 showed that the three ALK inhibitors have an open conformation of Pgp where the Ksv value was higher than that of apo-Pgp resulting in that conclusion.

In the absence of ligands, the X-ray crystal structure of P-gp shows that it is in the "open" conformation. The acrylamide quenching studies of Pgp with the ALK inhibitors and the non-

[53] Yang et al.

hydrolyzable ATP analog AMP-PNP in Fig. 3.5 show that ligand-induced alterations in tryptophan accessibility have a major impact on Pgp's tertiary conformation. Ligand-induced reductions in Pgp K_{SV} values reflect lower tryptophan accessibility and suggest a change toward a "closed" conformation for ceritinib and alectinib. Because the fluorescence quenching tests were performed with a non-hydrolyzable ATP analog rather than ATP, this information should be utilized with caution when assigning a specific drug- or nucleotide-bound Pgp conformation. Crizotinib on the other hand showed no significant changes in the Ksv value indicating no shift in the conformation of Pgp where it remained in the open confirmation. As a result, the conformational assignment was also based on Pgp-mediated ATP hydrolysis rates. In conclusion the acrylamide quenching tests of Pgp with the ALK inhibitors and the non-hydrolyzable ATP analog AMPPNP in vitro revealed ligand-induced alterations in tryptophan accessibility. These results suggest that their interactions significantly affect the tertiary conformation of Pgp.

REFERENCES

"202570s030lbl.Pdf." Accessed October 31, 2021. https://www.accessdata.fda.gov/drugsatfda_docs/label/2021/202570s030lbl.pdf.

"205755lbl.Pdf." Accessed October 31, 2021. https://www.accessdata.fda.gov/drugsatfda_docs/label/2014/205755lbl.pdf.

"208434s001lbl.Pdf." Accessed October 31, 2021. https://www.accessdata.fda.gov/drugsatfda_docs/label/2016/208434s001lbl.pdf.

"A Gene Optimization Strategy That Enhances Production of Fully Functional P-Glycoprotein in Pichia Pastoris," n.d.

Alexander, Stephen P. H., Alistair Mathie, and John A. Peters. "Guide to Receptors and Channels (GRAC), 5th Edition." *British Journal of Pharmacology* 164 Suppl 1 (November 2011): S1-324. https://doi.org/10.1111/j.1476-5381.2011.01649_1.x.

Al-Shawi, Marwan K., Mark K. Polar, Hiroshi Omote, and Robert A. Figler. "Transition State Analysis of the Coupling of Drug Transport to ATP Hydrolysis by P-Glycoprotein." *The Journal of Biological Chemistry* 278, no. 52 (December 26, 2003): 52629–40. https://doi.org/10.1074/jbc.M308175200.

Chifflet, S., A. Torriglia, R. Chiesa, and S. Tolosa. "A Method for the Determination of Inorganic Phosphate in the Presence of Labile Organic Phosphate and High Concentrations of Protein: Application to Lens ATPases." *Analytical Biochemistry* 168, no. 1 (January 1988): 1–4. https://doi.org/10.1016/0003-2697(88)90002-4.

Du, Xue, Yun Shao, Hai-Feng Qin, Yan-Hong Tai, and Hong-Jun Gao. "ALK-rearrangement in Non-small-cell Lung Cancer (NSCLC)." *Thoracic Cancer* 9, no. 4 (April 2018): 423–30. https://doi.org/10.1111/1759-7714.12613.

Friboulet, Luc, Nanxin Li, Ryohei Katayama, Christian C. Lee, Justin F. Gainor, Adam S. Crystal, Pierre-Yves Michellys, et al. "The ALK Inhibitor Ceritinib Overcomes Crizotinib Resistance in Non–Small Cell Lung Cancer." *Cancer Discovery* 4, no. 6 (June 1, 2014): 662–73. https://doi.org/10.1158/2159-8290.CD-13-0846.

Gutmann, Daniel A. P., Andrew Ward, Ina L. Urbatsch, Geoffrey Chang, and Hendrik W. van Veen. "Understanding Polyspecificity of Multidrug ABC Transporters: Closing in on the Gaps in ABCB1." *Trends in Biochemical Sciences* 35, no. 1 (January 2010): 36–42. https://doi.org/10.1016/j.tibs.2009.07.009.

Hrycyna, Christine A., Muralidhara Ramachandra, Suresh V. Ambudkar, Young Hee Ko, Peter L. Pedersen, Ira Pastan, and Michael M. Gottesman. "Mechanism of Action of Human P-Glycoprotein ATPase Activity: PHOTOCHEMICAL CLEAVAGE DURING A CATALYTIC TRANSITION STATE USING ORTHOVANADATE REVEALS CROSS-TALK BETWEEN THE TWO ATP SITES *." *Journal of Biological Chemistry* 273, no. 27 (July 3, 1998): 16631–34. https://doi.org/10.1074/jbc.273.27.16631.

Hurtado, Felipe K., Filippo de Braud, Javier De Castro Carpeño, Maria Jose de Miguel Luken, Ding Wang, Jeffrey Scott, Yvonne Y. Lau, Tracey McCulloch, and Morten Mau-Sorensen. "Effect of Ceritinib on the Pharmacokinetics of Coadministered CYP3A and 2C9 Substrates: A Phase I, Multicenter, Drug–Drug Interaction Study in Patients with ALK + Advanced Tumors." *Cancer Chemotherapy and Pharmacology* 87, no. 4 (April 1, 2021): 475–86. https://doi.org/10.1007/s00280-020-04180-3.

Juliano, R. L., and V. Ling. “A Surface Glycoprotein Modulating Drug Permeability in Chinese Hamster Ovary Cell Mutants.” *Biochimica Et Biophysica Acta* 455, no. 1 (November 11, 1976): 152–62. https://doi.org/10.1016/0005-2736(76)90160-7.

Lakowicz, Joseph R., ed. “Mechanisms and Dynamics of Fluorescence Quenching.” In *Principles of Fluorescence Spectroscopy*, 331–51. Boston, MA: Springer US, 2006. https://doi.org/10.1007/978-0-387-46312-4_9.

Lee, Jyh-Yeuan, Ina L. Urbatsch, Alan E. Senior, and Stephan Wilkens. “Projection Structure of P-Glycoprotein by Electron Microscopy. Evidence for a Closed Conformation of the Nucleotide Binding Domains.” *The Journal of Biological Chemistry* 277, no. 42 (October 18, 2002): 40125–31. https://doi.org/10.1074/jbc.M206871200.

Loo, Tip W., M. Claire Bartlett, and David M. Clarke. “Disulfide Cross-Linking Analysis Shows That Transmembrane Segments 5 and 8 of Human P-Glycoprotein Are Close Together on the Cytoplasmic Side of the Membrane.” *The Journal of Biological Chemistry* 279, no. 9 (February 27, 2004): 7692–97. https://doi.org/10.1074/jbc.M311825200.

Loo, Tip W., and David M. Clarke. “Drug-Stimulated ATPase Activity of Human P-Glycoprotein Is Blocked by Disulfide Cross-Linking between the Nucleotide-Binding Sites*.” *Journal of Biological Chemistry* 275, no. 26 (June 30, 2000): 19435–38. https://doi.org/10.1074/jbc.C000222200.

Cancer.Net. “Lung Cancer - Non-Small Cell - Statistics,” June 25, 2012. https://www.cancer.net/cancer-types/lung-cancer-non-small-cell/statistics.

Macdonald, Neil, and Alex Gledhill. “Potential Impact of ABCB1 (p-Glycoprotein) Polymorphisms on Avermectin Toxicity in Humans.” *Archives of Toxicology* 81, no. 8 (July 16, 2007): 553–63. https://doi.org/10.1007/s00204-007-0193-6.

Nandigama, Krishnamachary, Sabrina Lusvarghi, Suneet Shukla, and Suresh V. Ambudkar. “Large-Scale Purification of Functional Human P-Glycoprotein (ABCB1).” *Protein Expression and Purification* 159 (July 2019): 60–68. https://doi.org/10.1016/j.pep.2019.03.002.

Omote, Hiroshi, and Marwan Al-Shawi. “A Novel Electron Paramagnetic Resonance Approach to Determine the Mechanism of Drug Transport by P-Glycoprotein.” *The Journal of Biological Chemistry* 277 (December 1, 2002): 45688–94. https://doi.org/10.1074/jbc.M206479200.

Otterson, Gregory Alan, Gregory J. Riely, Alice Tsang Shaw, Lucio Crinò, Dong-Wan Kim, Renato Martins, Ravi Salgia, et al. “Clinical Characteristics of ALK+ NSCLC Patients (Pts) Treated with Crizotinib beyond Disease Progression (PD): Potential Implications for Management.” *Journal of Clinical Oncology* 30, no. 15_suppl (May 20, 2012): 7600–7600. https://doi.org/10.1200/jco.2012.30.15_suppl.7600.

“P-Glycoprotein - an Overview | ScienceDirect Topics.” Accessed December 10, 2021. https://www.sciencedirect.com/topics/pharmacology-toxicology-and-pharmaceutical-science/p-glycoprotein.

Qu, Qin, and Frances J. Sharom. “FRET Analysis Indicates That the Two ATPase Active Sites of the P-Glycoprotein Multidrug Transporter Are Closely Associated.” *Biochemistry* 40, no. 5 (February 1, 2001): 1413–22. https://doi.org/10.1021/bi002035h.

Robey, Robert W., Kristen M. Pluchino, Matthew D. Hall, Antonio T. Fojo, Susan E. Bates, and Michael M. Gottesman. “Revisiting the Role of ABC Transporters in Multidrug-Resistant Cancer.” *Nature Reviews. Cancer* 18, no. 7 (July 2018): 452–64. https://doi.org/10.1038/s41568-018-0005-8.

Romsicki, Y., and F. J. Sharom. “Phospholipid Flippase Activity of the Reconstituted P-Glycoprotein Multidrug Transporter.” *Biochemistry* 40, no. 23 (June 12, 2001): 6937–47. https://doi.org/10.1021/bi0024456.

Rosenberg, Mark F., Alhaji Bukar Kamis, Richard Callaghan, Christopher F. Higgins, and Robert C. Ford. “Three-Dimensional Structures of the Mammalian Multidrug Resistance P-Glycoprotein Demonstrate Major Conformational Changes in the Transmembrane Domains upon Nucleotide Binding *.” *Journal of Biological Chemistry* 278, no. 10 (March 7, 2003): 8294–99. https://doi.org/10.1074/jbc.M211758200.

Sakamoto, Hiroshi, Toshiyuki Tsukaguchi, Sayuri Hiroshima, Tatsushi Kodama, Takamitsu Kobayashi, Takaaki A. Fukami, Nobuhiro Oikawa, Takuo Tsukuda, Nobuya Ishii, and Yuko Aoki. “CH5424802, a Selective ALK Inhibitor Capable of Blocking the Resistant Gatekeeper Mutant.” *Cancer Cell* 19, no. 5 (May 17, 2011): 679–90. https://doi.org/10.1016/j.ccr.2011.04.004.

Sarkadi, B., E. M. Price, R. C. Boucher, U. A. Germann, and G. A. Scarborough. “Expression of the Human Multidrug Resistance CDNA in Insect Cells Generates a High Activity Drug-Stimulated Membrane ATPase.” *The Journal of Biological Chemistry* 267, no. 7 (March 5, 1992): 4854–58.

Sharom, F. J., X. Yu, and C. A. Doige. “Functional Reconstitution of Drug Transport and ATPase Activity in Proteoliposomes Containing Partially Purified P-Glycoprotein.” *The Journal of Biological Chemistry* 268, no. 32 (November 15, 1993): 24197–202.

Shaw, Alice T., Dong-Wan Kim, Kazuhiko Nakagawa, Takashi Seto, Lucio Crinó, Myung-Ju Ahn, Tommaso De Pas, et al. “Crizotinib versus Chemotherapy in Advanced ALK-Positive Lung Cancer.” *The New England Journal of Medicine* 368, no. 25 (June 20, 2013): 2385–94. https://doi.org/10.1056/NEJMoa1214886.

Shilling, Richard A., Henrietta Venter, Saroj Velamakanni, Akanksha Bapna, Barbara Woebking, Sanjay Shahi, and Hendrik W. van Veen. “New Light on Multidrug Binding by an ATP-Binding-Cassette Transporter.” *Trends in Pharmacological Sciences* 27, no. 4 (April 1, 2006): 195–203. https://doi.org/10.1016/j.tips.2006.02.008.

“Unravelling the Complex Drug–Drug Interactions of the Cardiovascular Drugs, Verapamil and Digoxin, with P-Glycoprotein | Bioscience Reports | Portland Press.” Accessed October 31, 2021. https://portlandpress.com/bioscirep/article/36/2/e00309/56248/Unravelling-the-complex-drug-drug-interactions-of.

Wang, R. B., C. L. Kuo, L. L. Lien, and E. J. Lien. “Structure–Activity Relationship: Analyses of p-Glycoprotein Substrates and Inhibitors.” *Journal of Clinical Pharmacy and Therapeutics* 28, no. 3 (2003): 203–28. https://doi.org/10.1046/j.1365-2710.2003.00487.x.

Wilt, Laura A., Diana Nguyen, and Arthur G. Roberts. “Insights into the Molecular Mechanism of Triptan Transport by P-Glycoprotein.” *Journal of Pharmaceutical Sciences* 106, no. 6 (June 2017): 1670–79. https://doi.org/10.1016/j.xphs.2017.02.032.

Yang, Ke, Yifan Chen, Kenneth Kin Wah To, Fang Wang, Delan Li, Likun Chen, and Liwu Fu. “Alectinib (CH5424802) Antagonizes ABCB1- and ABCG2-Mediated Multidrug Resistance in Vitro, in Vivo and Ex Vivo.” *Experimental & Molecular Medicine* 49, no. 3 (March 2017): e303–e303. https://doi.org/10.1038/emm.2016.168.

Zhou, S.-F. “Structure, Function and Regulation of P-Glycoprotein and Its Clinical Relevance in Drug Disposition.” *Xenobiotica; the Fate of Foreign Compounds in Biological Systems* 38, no. 7–8 (July 2008): 802–32. https://doi.org/10.1080/00498250701867889.

Zhou, Wen-jing, Xu Zhang, Chao Cheng, Fang Wang, Xiao-kun Wang, Yong-ju Liang, Kenneth Kin Wah To, Wang Zhou, Hong-bing Huang, and Li-wu Fu. “Crizotinib (PF-02341066) Reverses Multidrug Resistance in Cancer Cells by Inhibiting the Function of P-Glycoprotein.” *British Journal of Pharmacology* 166, no. 5 (2012): 1669–83. https://doi.org/10.1111/j.1476-5381.2012.01849.x.